Article

Current Biology

Inverse Control of Turning Behavior by Dopamine D1 Receptor Signaling in Columnar and Ring Neurons of the Central Complex in *Drosophila*

Highlights

- Freely moving *Drosophila* present preferred patterns of activity and turning behavior
- *FoxP* mutations affect temporal distribution of motor actions and turning behavior
- Central complex columnar E-PG and R2/4 m ring neurons inversely regulate turning
- Dopamine D1-like receptor signaling in R2/R4m ring neurons modulates behavior

Authors

Benjamin Kottler, Richard Faville, Jessika Cristina Bridi, Frank Hirth

Correspondence

benjamin.kottler@kcl.ac.uk (B.K.), frank.hirth@kcl.ac.uk (F.H.)

In Brief

Kottler et al. use a novel behavioral paradigm to show that dopamine D1-like receptor Dop1R1 signaling in columnar E-PG and ellipsoid body R2/R4m ring neurons mediate temporal patterns of activity and inversely control turning, suggesting that Dop1R1 levels between interconnected central complex circuitry modulate behavioral performance in flies.

Kottler et al., 2019, Current Biology *29*, 567–577
February 18, 2019
https://doi.org/10.1016/j.cub.2019.01.017

CellPress

Current Biology
Article

Inverse Control of Turning Behavior by Dopamine D1 Receptor Signaling in Columnar and Ring Neurons of the Central Complex in *Drosophila*

Benjamin Kottler,[1,*] Richard Faville,[1] Jessika Cristina Bridi,[1] and Frank Hirth[1,2,*]
[1]Department of Basic & Clinical Neuroscience, Institute of Psychiatry, Psychology & Neuroscience, Maurice Wohl Clinical Neuroscience Institute, King's College London, London, UK
[2]Lead Contact
*Correspondence: benjamin.kottler@kcl.ac.uk (B.K.), frank.hirth@kcl.ac.uk (F.H.)
https://doi.org/10.1016/j.cub.2019.01.017

SUMMARY

Action selection is a prerequisite for decision-making and a fundamental aspect to any goal-directed locomotion; it requires integration of sensory signals and internal states to translate them into action sequences. Here, we introduce a novel behavioral analysis to study neural circuits and mechanisms underlying action selection and decision-making in freely moving *Drosophila*. We discovered preferred patterns of motor activity and turning behavior. These patterns are impaired in *FoxP* mutant flies, which present an altered temporal organization of motor actions and turning behavior, reminiscent of indecisiveness. Then, focusing on central complex (CX) circuits known to integrate different sensory modalities and controlling premotor regions, we show that action sequences and turning behavior are regulated by dopamine D1-like receptor (Dop1R1) signaling. Dop1R1 inputs onto CX columnar ellipsoid body-protocerebral bridge gall (E-PG) neuron and ellipsoid body (EB) R2/R4m ring neuron circuits both negatively gate motor activity but inversely control turning behavior. Although flies deficient of D1 receptor signaling present normal turning behavior despite decreased activity, restoring Dop1R1 level in R2/R4m-specific circuitry affects the temporal organization of motor actions and turning. We finally show EB R2/R4m neurons are in contact with E-PG neurons that are thought to encode body orientation and heading direction of the fly. These findings suggest that Dop1R1 signaling in E-PG and EB R2/4 m circuits are compared against each other, thereby modulating patterns of activity and turning behavior for goal-directed locomotion.

INTRODUCTION

Action selection is the process to ''do the right thing at the right time'' [1]. It is a prerequisite for decision-making underlying goal-directed locomotion [2], which requires the integration of sensory signals with internal states to translate them into action sequences. The most basic action selection for any ambulatory animal is between action and inaction, movement and immobility. Once activity is initiated, the sequence of activity bouts necessitates their correct organization into action sequences (Figure 1A). Although speed can vary, moving from a starting point to a specific destination can be achieved by either one single bout or several successive bouts of activity. Moreover, the distribution of activity bouts can follow a scale-invariant pattern [3]. It has been shown that animals, from human to fly, have a tendency to initiate movement in bursts of activity rather than randomly. This is illustrated by the distribution of inter-bout intervals (IBIs) or pauses between two activity periods, also called inter-activity intervals [4], which can follow a non-stochastic pattern, characterized by burstiness [3–5]. But goal-directed locomotion also includes decision-making processes that can be best summarized by ''you can't turn left and right at the same time.'' When an animal is moving toward an obstacle, a decision is necessary to avoid collision [2] and a turn has to be executed (Figure 1D). Therefore, a selection between available alternatives needs to be made regarding the nature of the turn either by stopping and remaining inactive or by changing direction by turning left or right.

In flies and other insects, several lines of evidence suggest that the central complex (CX) is involved in action selection and decision-making processes. The CX integrates various sensory cues and orchestrates motor output for adaptive behavioral manifestations, which range from sleep, arousal, and attention to higher motor control, including goal-directed locomotion, orientation tuning, path integration, and place learning [6–13]. The CX is a central brain structure composed of midline neuropils comprising the protocerebral bridge (PB), the fan-shaped body (FB), the ellipsoid body (EB), and the noduli, together which are connected to the lateral accessory lobes (LAL) that are part of the lateral complex. Two major types of projection neurons characterize the circuit architecture of the CX. On the one hand, columnar neurons interconnect the different substructures of the CX, from PB to EB [14–16], and compartmentalize them into segments or modules, each of which corresponds to a segment of sensory space [7, 17]. Different types of columnar neurons have been characterized, among them ellipsoid body-protocerebral bridge gall (E-PG) [18] and protocerebral bridge-ellipsoid body noduli (P-EN) neurons [19]. Several studies propose that visual cues and their position in space are

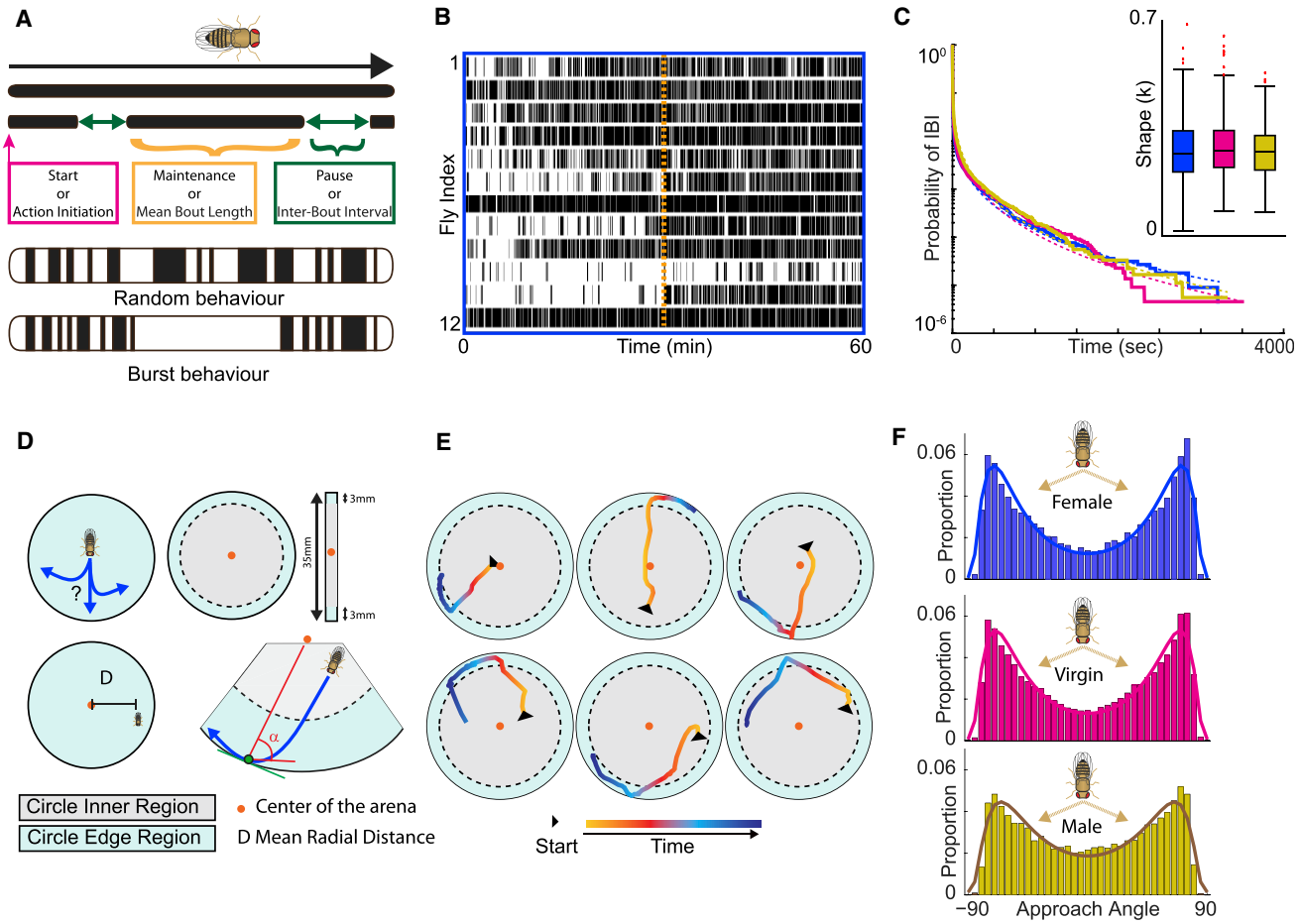

Figure 1. Open-Field Behavior of Freely Moving Control Flies

(A) Temporal sequence of activity bouts and inter-bout intervals (IBIs). Each activity bout is characterized by three main components: a start (pink square) that initiates an activity bout; a mean bout length (gold) or duration that represents its maintenance; and an IBI (in green) that corresponds to the pause in between the stop and start of two consecutive activity bouts; activity can follow a random distribution or burstiness where bouts of activity are clustered.

(B) Raster plot of activity bouts (black bars) and IBIs (white) of 12 randomly chosen female flies; the dashed vertical orange line represents the mechanical stimuli applied after 30 min of recording.

(C) Weibull plot of mean IBI distribution over time revealing a heavy tail—meaning that there is a larger probability of getting large values; inset graph depicts shape factor κ, which is a measure of random behavior (=1) versus burstiness (<1); values are shown for three w^{1118} control groups: females (blue); virgins (pink); and males (yellow).

(D) Open-field arena divided into inner region (gray) and edge region (blue) delimited by 3 mm distance from the edge; red dot represents arena centroid. The approach angle α is the deviation between the trajectory of the fly (in blue) when entering the edge region until contact with the wall (green dot) and the perpendicular at the point of contact to the centroid of the arena.

(E) Six examples of turning flies.

(F) Approach angle distribution for w^{1118} control groups, females, virgins, and males reveals bimodal distribution of turns with peaks at ±65°–70°.

See also Figure S1 and Data S1.

represented in EB activity relative to the animal's heading. *In vivo* calcium-imaging studies using GCaMP6f expressed in E-PG neurons identified a bump of activity restricted to a segment of the EB as an internal representation of the angular orientation of an individual fly [18, 20]. These results suggest that E-PG neuron activity encodes an internal compass and heading direction that combines visual landmarks with self-generated (idiothetic) cues [21, 22] necessary for proper navigation [23]. On the other hand, tangential neurons form synaptic layers of the FB and EB. Among other behavioral manifestations, such as a role for sleep and arousal [24–26], tangential EB ring neurons relay visual cues from the bulbs to the EB [18] and have been implicated in the regulation of visual place learning and visual orientation memory [27, 28]. Together, these data suggest that E-PG and tangential ring neuron circuits converge onto the EB, leading to the integration of self-generated cues and external sensory cues, two features essential for correct navigation. However, despite detailed anatomical and physiological studies into CX functions, the neural mechanisms and molecular substrates mediating action selection and decision-making related to goal-directed locomotion are only starting to emerge.

Here, using a novel behavioral analysis, we investigated the organization of motor activity and turning behavior in freely moving *Drosophila* and identified a preferred pattern of temporal

activity and turning behavior. We validated our approach by analyzing well-described mutants of the forkhead box transcription factor gene, *FoxP*, that are impaired in decision-making [29–31]. Analysis of their locomotion revealed that, independently of activity levels, these *FoxP* mutants present variation in the distribution of IBIs and impaired turning behavior.

We then applied our novel paradigm to investigate the role of CX circuitry in action selection and decision-making. We show that D1 dopamine receptor Dop1R1 activity regulates turning behavior both in E-PG and tangential EB ring neurons. Synaptically targeted GFP reconstitution across synaptic partners (GRASP) identified reciprocal connections between these two circuits. Manipulations of Dop1R1 levels in R2/R4m, but not other ring neuron circuitry in wild-type and in a Dop1R1 heterozygote mutant background, $dumb^2$, revealed a specific role of the outer EB ring circuit for D1 receptor signaling in mediating turning. Our results demonstrate that CX circuit activity coordinates not only the temporal sequence of motor actions but also turning behavior. Moreover, they suggest that the ratio of dopamine D1 receptor signaling between E-PG and EB R2/R4m neurons mediates their correct execution.

RESULTS

Freely Moving Flies Show Preferred Temporal Patterns of Activity and Turning Behavior

To investigate motor action selection, we recorded the activity of freely moving flies in 35-mm-diameter arenas for 1 h. Using the *Drosophila* arousal tracking (DART) system [32] (Figure S1A), we quantified motor action sequences and movement trajectories (Figures 1B and 1E). Additionally, as a measure for the arousal state of a fly, we determined the response to sensory stimulation triggered by mechanical vibrations (Figure S2E). We first tested our system by recording the activity of w^{1118} mated female, virgin female, and mated male control flies at 25°C and determined their temporal sequence of activity (respectively labeled in blue, pink, and yellow in Figures 1 and S1). Fly motor activity can be represented as a raster plot, where each bout of activity is indicated by black lines (Figure 1B). Because animal activity is characterized by burstiness [3–5], we also investigated the distribution of IBIs across the 60-min window of recording. Similar to experiments that recorded activity over several days [4], we found that the complementary cumulative distribution of IBIs fitted with the complementary cumulative Weibull distribution for all control groups (Figure 1C). Weibull distributions are characterized by the scale parameter κ that reflects the degree of burstiness (Figure 1C). A scale parameter κ of 1 corresponds to a random distribution (Poisson) of IBIs, and its decrease corresponds to an increase in burstiness. For all control groups, we observed scale factors κ lower than 1, suggesting that, even during 60 min recording, the temporal pattern of motor action sequences in *Drosophila* follows a non-stochastic distribution characterized by bursts of activity, with periods of burst activity separated by longer pause.

In parallel, we developed a paradigm to investigate turning behavior as a proxy for decision-making. While freely moving in an open arena, flies tend to avoid the center, a behavior termed "centrophobism" [33]. Despite their tendency to follow the wall, flies leave the edge to explore the central zone of the arena, after which, they return to the edge again. Thus, when re-approaching the edge of the arena, flies have to make a decision in order to avoid a collision with the wall, by achieving a turn that we can calculate. For that purpose, we divided the arena into two regions: the inner (center) region and the edge (wall) region (Figure 1D, light gray and light blue, respectively), with the edge region defined by a 3-mm distance width, which is at least twice as long as the body length of a fly. We then determined the mean radial distance for all control groups, which is the mean distance of a fly from the center of the arena. We showed that their movement was circumscribed at the arena edge region. This allowed us to determine their place preference pictured with a heatmap representation, which captures the percentage of time spent in the inner and outer region and the transitions between inner or center to outer or edge region (Figure S1B). For the turning behavior analysis, we specifically investigated turning events of flies transitioning from the inner region to the edge region within a continuous bout of activity (STAR Methods). This restrictive definition allowed us to analyze necessary turns representing an inherent decision-making event, even when perceptual choices were not obvious (Figure 1E). We calculated the deviation angle between the fly's trajectory and the perpendicular of the asymptote at the point of contact with the wall (denoted α in Figures 1D and S1C). These deviation angles could range from $-90°$ and $+90°$, with a value of $0°$ representing a straight walk to the wall of the arena. Analysis of the proportional distribution of these approach angles for control flies revealed a bimodal distribution of turns, with the most common modes or angles being around the absolute value of $\pm70°$–$80°$ (Figure 1F). This bimodal distribution was extremely robust across gender, age, and time of day (Figure S1D). Together, these results suggest that, in addition to a non-stochastic temporal distribution of activity bouts, fly turning behavior in a circular open arena follows a spatial pattern with preferred angles of approach, characteristic of a bimodal distribution.

FoxP Mediates Motor Action Sequences and Turning Behavior

In order to validate that our behavioral analysis can be used for studying action selection and decision-making, we first analyzed *FoxP* mutants. *Drosophila* FoxP encodes a homolog of the FoxP2 transcription factor, which when mutated affects the temporal sequence of vocalizations in human, mice, and songbirds [34, 35]. So far, three different *FoxP* isoforms have been identified in the fruit fly, which differ in their binding sequence [31]. The two *FoxP* mutants used in our study, $FoxP^{5\text{-}SZ\text{-}3955}$ and $FoxP^{f03746}$, are distinct with respect to expression of the different isoforms. $FoxP^{f03746}$ only present an elevated isoform A, and $FoxP^{5\text{-}SZ\text{-}3955}$ does not show any significant difference in any of the isoforms except that the putative isoform B is truncated [31]. Previous studies using the fruit fly revealed that *FoxP* mutants exhibit a defect in an operant self-learning, but not in a world-learning assay [31]. This difference indicates that *FoxP* mutants are defective to assign value to self-generated actions, but not for the assessment of external sensory cues. Previous studies also showed delayed decision-making in an odor-discrimination task suggestive of indecision [29, 36]. We used two previously characterized *FoxP* mutants, $FoxP^{5\text{-}SZ\text{-}3955}$ and $FoxP^{f03746}$, and compared their behavior with w^{1118} control flies

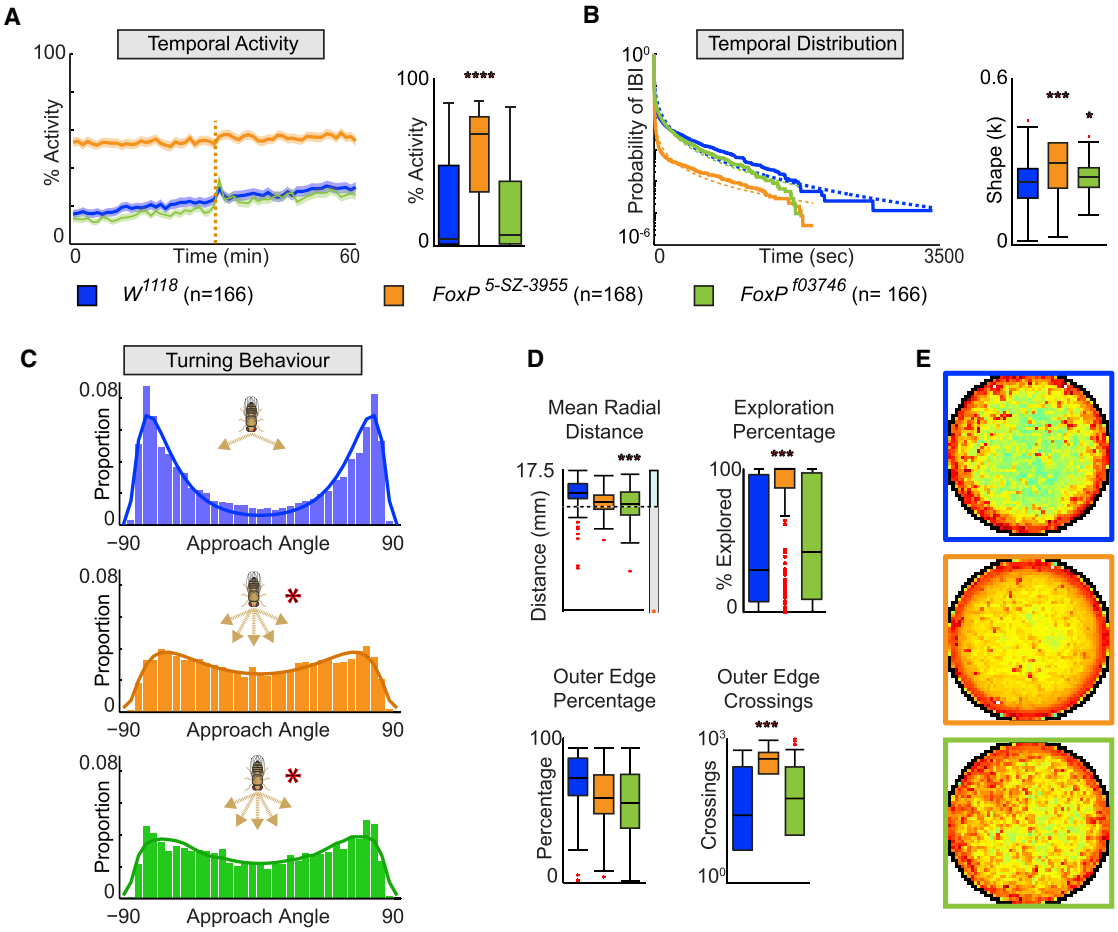

Figure 2. Locomotor Kinematics and Open-Field Behavior of Freely Moving *FoxP* Mutant Flies

(A) Analysis of $FoxP^{5\text{-}SZ\text{-}3955}$ (orange) and $FoxP^{f03746}$ (green) mutant flies compared to w^{1118} control (blue).

(B) Temporal activity over 1-h recording with shaded area representing SEM—which was used to indicate the precision of the estimate of the mean; dashed vertical line represents mechanical stimuli applied after 30 min of recording; right panel, mean activity over 60 min.

(C) Temporal distribution of IBIs fitted to a Weibull distribution and the dotted line showing the survival curve fitted response; right panel, shape factor κ.

(D) Turning behavior with approach angle. The fly cartoon represents bimodal distribution that is impaired in *FoxP* mutants.

(E) Mean radial distance during turns (top left), mean exploration behavior covering arena space (top middle), place preference shown as heatmap (right), percentage spent in outer edge region (bottom left), and mean number of crossings between inner region and outer edge region (bottom middle). All data are mean ± SEM; *p < 0.5; **p < 0.01; ***p < 0.001.

See also Figure S2 and Data S1.

[29, 31, 36]. Whereas the two *FoxP* mutants clearly presented different levels of activity and active speed (Figures 2A and S2C–S2E with $FoxP^{5\text{-}SZ\text{-}3955}$ and $FoxP^{f03746}$, respectively, in orange and green), they both exhibited a similar decrease in burstiness, as illustrated by the increased shape factor κ compared to control (Figure 2B), indicative of defective action selection processing [4].

Next, we determined the turning behavior of these *FoxP* mutants, which identified a common behavioral difference compared to the control. Although w^{1118} flies showed a strong bimodal distribution of turns with peaks around ±70°–80°, the two *FoxP* mutants revealed a more flattened distribution (Figure 2C). These alterations in the distribution of the approach angle could not be attributed to differences in place preference, as the 2D heatmap still highlighted centrophobism (Figure 2D). Moreover, the mean radial distances for both mutants were above the separation between inner and edge regions, even though $FoxP^{f03746}$ mutants were further away from the edges as depicted by the decrease in the radial distance (Figure 2D). More importantly, neither of these two *FoxP* mutants showed any differences in the percentage of time spent in the outer edge region despite differences in both exploration and the absolute number of crossings for $FoxP^{5\text{-}SZ\text{-}3955}$, which could be attributed to its higher activity level. We do not think these differences could be attributed to some locomotor defect impacting the capacity of turning, as active speed for $FoxP^{5\text{-}SZ\text{-}3955}$ and distance traveled post-contact for both mutants were not different from the control (Figures S2B and S2D). In line with previous findings [29, 31], these data support a role for *FoxP* in motor control and decision-making and disentangle activity levels from burstiness and turning, suggesting that these behavioral manifestations are regulated by different mechanisms and/or neural circuits.

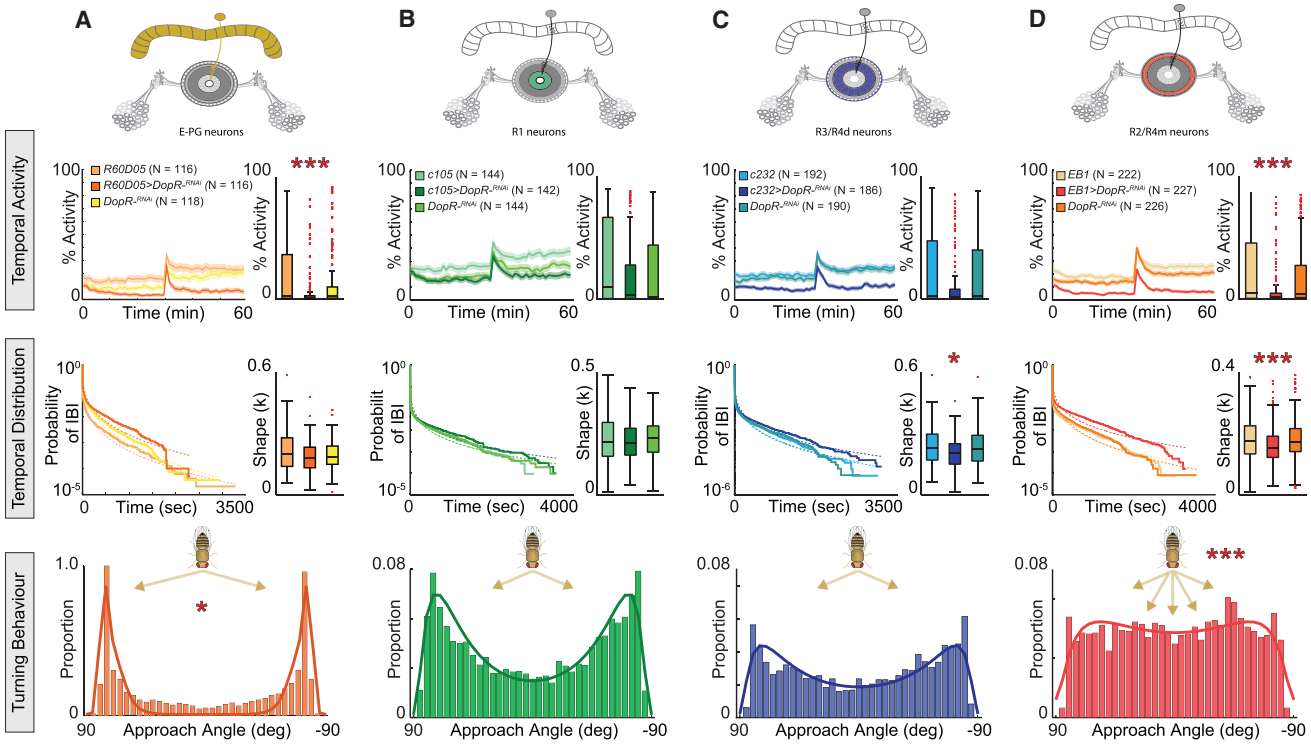

Figure 3. E-PG and Tangential Ring Neurons Differentially Modulate Motor Activity and Turning Behavior via Circuit-Specific D1 Receptor Signaling

Color-coded Gal4 expression pattern schematics for *UAS-Dop1R1*$^{-RNAi}$ expression by (A) *R60D05-Gal4* targeting E-PG neurons (orange), (B) *c105-Gal4* targeting ellipsoid body (EB) R1 circuitry (green), (C) *c232-Gal4* targeting R3/R4d circuitry (blue), (D) *EB1-Gal4* targeting R2/R4m circuitry (red), and their respective controls (*Gal4*/+ and *UAS*/+). Temporal activity resolution is shown with the shaded area representing the SEM and activity percentage over the recorded hour. All data are mean ± SEM; *p < 0.5, **p < 0.01, ***p < 0.001. See also Figure S3 and Data S1.

Dopamine D1-like Receptor Signaling in E-PG Neurons Modulates Motor Activity and Turning Behavior

Modulatory dopamine receptor signaling is a key feature of action selection circuitries [9, 37]. In *Drosophila*, *Dop1R1* encodes a D1-like dopamine receptor that has been shown to be expressed in the CX [38, 39] and is required for a wide range of behavioral manifestations ranging from learning and memory to sleep and arousal [40–43]. To study D1 function in our paradigm, we first examined whether its activity in E-PG neurons may regulate motor action sequences and turning behavior. Activity of E-PG neurons has been shown to represent a heading direction [20, 44]. Heading direction signals are required for correct spatial navigation, which is manifested in successive motor action sequences, including turns. We therefore hypothesized that targeted manipulation of D1 activity in E-PG neurons may impair motor action sequences and turning behavior.

To test this, we used the previously [19, 20] characterized R60D05-*Gal4* driver specific to E-PG neurons (Figure S3A) and expressed *UAS-Dop1R1*$^{-RNAi}$ to impair D1 signaling. This RNAi construct potently reduces Dop1R1 levels when expressed in brain neurons of adult *Drosophila* [45]. R60D05-Gal4 > Dop1R1^{-RNAi} flies revealed significantly decreased activity levels but did not show alterations in burstiness. Interestingly, their approach angle distribution was statistically accentuated toward ±75° angles and thus more pronounced compared to controls (Figure 3A). Detailed analysis of R60D05 > Dop1R1^{-RNAi} flies also revealed decreased centrophobism, even though they statistically explored less, probably due to the lowered activity level. In fact, they proportionally spent less time in the edge region, which might be indicating that their perception of the open arena could have been altered (Figure S3A).

EB R2/R4m Circuit-Specific Dop1R1 Function Regulates Temporal Activity Patterns and Turning Behavior

We next studied tangential EB ring neurons and hypothesized that their dysfunction could affect the temporal pattern of motor actions and/or turning behavior. To test this proposition, we used three Gal4 driver lines that have been widely used to characterize roles of EB R1–4 neurons in spatial orientation and place learning [18, 28, 46, 47]. *c105-Gal4* shows expression in the inner ring layer (R1), *c232-Gal4* targets the middle (R3) and outer (or distal) rim layer (R4d), and *EB1-Gal4* drives expression in the median and outer layers (R2 and R4m; Figures S3B–S3D). Thus, we examined the role of Dop1R1 by downregulating its expression in R1–4 ring neuron circuitries.

Expression of *UAS-Dop1R*$^{-RNAi}$ in R1 and R3/R4d layers, using c105 and c232 Gal4 driver lines, respectively, did not modify activity levels (Figures 2B and 2C). A slight but statistically not significant decrease could be observed with the *c232-Gal4* driver (Figure 3C). This was accompanied with less exploration and the flies being significantly closer to the edge (Figures S3B and S3C). Interestingly, burstiness was altered in *c232-Gal4* >

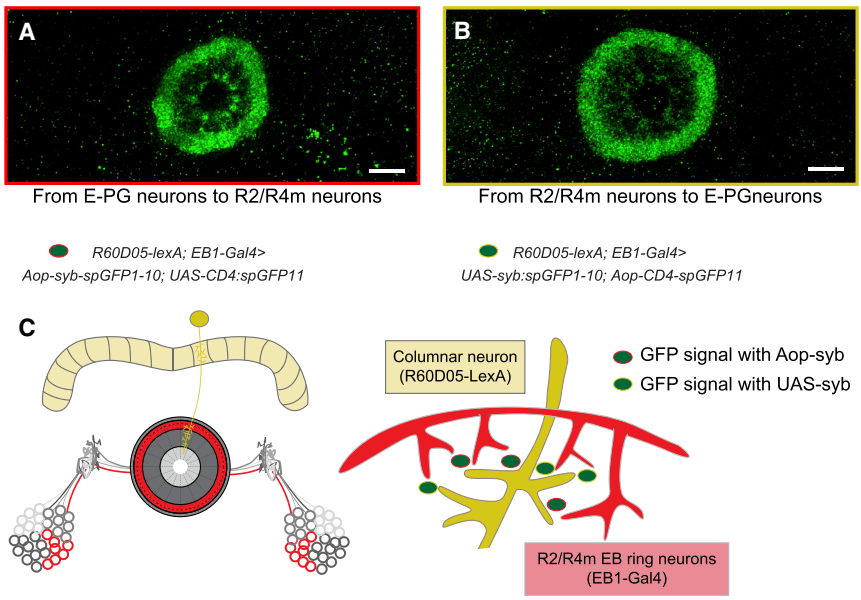

Figure 4. Synaptobrevin-Tagged GFP Reconstitution across E-PG and Tangential Ring Neurons

R60D05-lexA is specific for E-PG neurons and *EB1-Gal4* specific for tangential ring neurons.

(A) *R60D05-lexA; EB1-Gal4 > Aop-syb-spGFP1-10; UAS-CD4:spGFP11* visual reconstruction of GFP signal obtained with Aop-syb-tagged GFP fragments (indicative of contact from columnar to tangential neurons).

(B) *R60D05-lexA; EB1-Gal4 > UAS-syb::spGFP1-10;Aop-CD4-spGFP11* indicate GFP signal obtained with UAS-syb-tagged GFP fragments (suggesting contact from tangential to columnar neurons).

(C) Schematic of contact between columnar and R2.R4m tangential neurons on to the EB. Green dots with red frame indicate GFP signal obtained with Aop-syb-tagged GFP fragments as in (A); green dots with yellow frame indicate GFP signal obtained with UAS-syb-tagged GFP fragments as in (B). Scale bars 20 μm.

See also Figure S4 and Data S1.

Dop1R^{-RNAi} (Figure 3C), and a trend toward a less pronounced turning behavior could be observed, which was not significantly different from the controls. Remarkably, driving *UAS-Dop1R*$^{-RNAi}$ with the R2/R4m driver line *EB1-Gal4* led to a severe decrease in overall activity, which was accompanied with increased burstiness as revealed by the decreased κ factor compared to controls (Figure 3D). Similar to R3/R4d-specific manipulations with *c232-Gal4*, *EB1-Gal4 > Dop1R*$^{-RNAi}$ flies were more centrophobic and explored less the arena. Moreover, this R2/R4m-specific overexpression of *UAS-Dop1R*$^{-RNAi}$ with the *EB1-Gal4* driver resulted in a change in the distribution of the angular approach, which no longer showed the typical bimodal distribution (Figure 3D). These data identify that E-PG and EB R2/R4m neurons negatively gate motor activity and that EB R2/R4m circuit-specific D1 signaling modulates the correct organization of motor actions and turning behavior.

E-PG Neurons Are Reciprocally Connected with Tangential Ring Neurons

Given the striking opposite turning behavior phenotypes mediated by E-PG and R2/R4m ring neurons, we wondered whether this might be due to functional interaction between these circuits. As already suggested by previous studies [2, 24], we postulated that E-PG neurons would be connected with EB ring neuron circuitry and that ring neurons mediate motor action selection.

In order to test this hypothesis, we used the GRASP system to visualize potential synaptic connections between E-PG and tangential ring neurons. GRASP utilizes the expression of two split-GFP halves that only fluoresce when reconstituted [48]. We applied a synaptically targeted GRASP system (syb-GRASP) [49] and used EB1-Gal4 specific to tangential R2/R4m ring neurons together with the R60D05-LexA driver specific to E-PG neurons (Figure S4).

We utilized split-GFP fragments Aop-CD4::spGFP11 and *UAS*-syb::spGFP1-10 that allow visualization of connections from ring to column, whereas a combination of Aop-syb::spGFP1-10 and *UAS*-CD4::spGFP11 allowed to visualize connections from column to ring. When combined, we detected GFP fluorescence around the circumference of the EB R2/R4m layer, restricted to predicted interactions of both singular expression patterns (Figures 4A and 4B). This GFP signal occurred in any combination indicative of potential reciprocal cell contacts between E-PG and ring neurons (Figure 4C), as previously predicted by computational interrogation for goal-directed locomotion [2] and CX circuit activity encoding heading direction [50].

D1-like Receptor Signaling in EB R2/R4m Circuitry Regulates Motor Action Sequences and Turning Behavior

In order to gain further insights into EB Dop1R1-mediated action selection and decision-making mechanisms, we investigated *Dop1R1* mutant flies. *Dumb*^{2}, or *DopR*^{f02676}, is a well-characterized strong hypomorphic allele [25] that results in deficient learning and memory formation but also impairs arousal, sleep, as well as goal-directed and ethanol-induced locomotion [38, 40–43]. Specifically, the *dumb*^{2} mutation is caused by a P-element insertion in the first intronic region of the *Dop1R* gene [40], resulting in a dramatic decrease of Dop1R protein levels [25]. This P-element contains an upstream activating sequence (UAS) cassette to which the Gal4 transcriptional activator can bind. By crossing the *dumb*^{2} mutant with a selective Gal4 driver, we can specifically restore Dop1R1 expression in neuronal subsets and circuits defined by the spatio-temporal activity of the respective Gal4 driver. In addition, this mutation does not show any compensatory effect on transcript levels for the DA receptors Dop1R2 and D2R [41].

We compared the *dumb*^{2} mutant with our control *w*^{1118} flies. At our level of resolution and timescale of analysis, we observed a significant decrease of activity. *dumb*^{2} mutant flies showed an altered temporal pattern of activity with increased burstiness

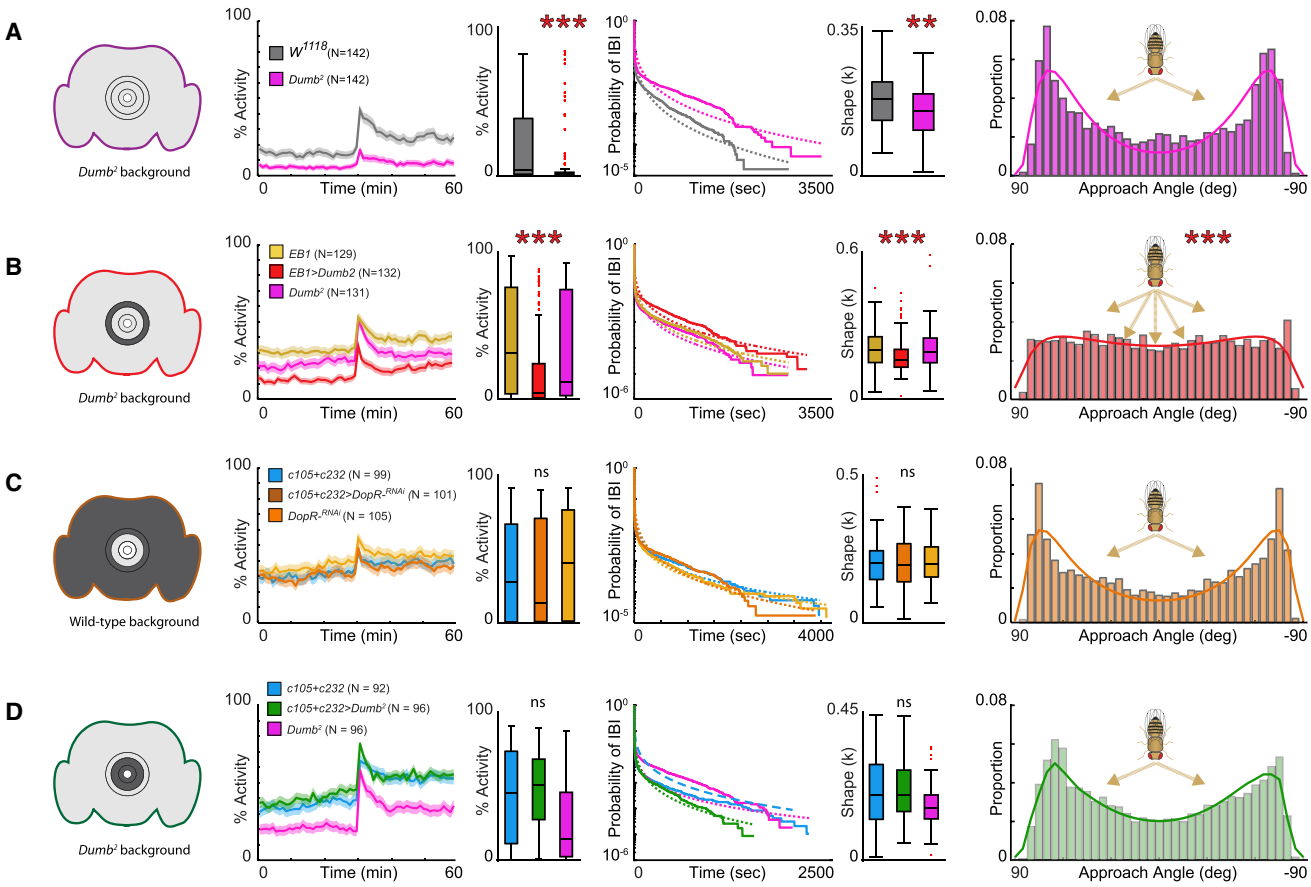

Figure 5. Dop1R1 Receptor Imbalance in Ellipsoid Body R2/R4m Circuit Affects Temporal Distribution of Activity Bouts and Turning Behavior

Panels from left to right indicate Dop1R1 levels in entire brain and/or ring neuron subtype-specific ellipsoid body (EB) circuitry, temporal activity levels with shaded area representing SEM, mean activity, temporal distribution of inter-bout intervals (IBIs), shape factor κ, and distribution of approach angle for (A) *Dumb²* mutant compared to w^{1118} control flies, (B) R2/R4m-specific *EB1-Gal4* targeting Dop1R1 in *Dumb²* heterozygous background, (C) R1+R3/4d-specific *c105+c232-Gal4* expression of *UAS-Dop1R1-RNAi*, and (D) R1+R3/4d-specific *c105+c232-Gal4* targeting Dop1R1 in *dumb²* heterozygous background. All data are mean ± SEM; *p < 0.5; **p < 0.01; ***p < 0.001. See also Figures S5 and S6 and Data S1.

revealed by the decreased shape factor κ, confirming earlier findings that dopamine levels affect burstiness [4]. Interestingly, the behavior of *dumb2* mutant flies was also characterized by reduced centrophobism (Figure S6A), indicative of altered place preference. However, the turning behavior of *dumb²* mutant flies still revealed a bimodal distribution (Figure 5A). This surprising result suggests that efficient turning behavior does not rely on overall dopamine D1 receptor level but rather that Dop1R1 signaling in E-PG and EB R2/4 m circuits is compared against each other. Restoring Dop1R1 level in *dumb²* heterozygous background in E-PG neurons with R60D05-Gal4 or in the R1 or R3/4d layers with c105 and c232 driver lines, respectively, did not cause changes in the pattern of burstiness or the approach angle distribution (Figures S5A–S5C). In contrast, activity levels were affected by selectively restoring Dop1R1 level in the R2/R4m circuit with the *EB1-Gal4* driver in *dumb²* heterozygous background. *EB1-Gal4 > UAS-dumb²* flies were also characterized by increased burstiness illustrated by the decreased shape factor κ. Moreover, the bimodal distribution of turns was no longer detectable in *EB1-Gal4 > UAS-dumb²* flies (Figures 5B and S6B). These results pointed to a specific requirement of Dop1R1 signaling in R2/R4m circuitry. To further substantiate this observation, we selectively targeted Dop1R1 level in R1, R3, and R4d together by combining *c105-Gal4* and *c232-Gal4*, by downregulating Dop1R1 level in wild-type background, but also by restoring its Dop1R1 levels in *dumb²* heterozygotes background (Figures 5C and 5D). Downregulating Dop1R1 in a wild-type background together with *c105-Gal4* and *c232-Gal4* did not affect any behavior endpoint (Figures 6C and S6C). In contrast, restoring Dop1R1 level in the *dumb²* heterozygotes background together with *c105-Gal4* and *c232-Gal4* resulted in reduced centrophobism and enhanced exploration (Figure S6D), indicative of altered place preference. However, neither the temporal organization of motor actions nor turning behavior was affected as *c105-Gal4 > UAS-dumb²*, *c232-Gal4 > UAS-dumb²*, *c105-Gal4-c232-Gal4 > UAS-dumb²*, and *c105-Gal4-c232-Gal4 > Dop1R-RNAi* flies were not statistically different from both parental controls—even though *dumb²* was. Together, these results identify an EB R2/R4m circuit-specific requirement of Dop1R1 in the regulation of motor activity and turning behavior in *Drosophila*.

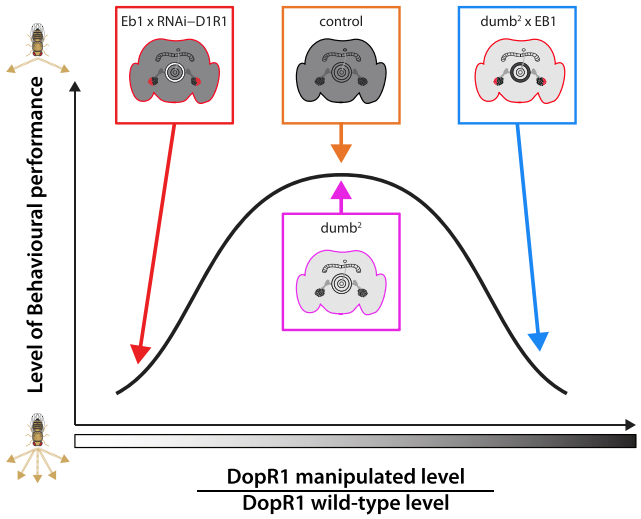

Figure 6. Proposed Model for Dop1R1 Requirement in the CX for Turning Behavior

The observed findings indicate that dopamine D1 receptor signaling modulates E-PG and EB R2/4 m circuit activities, which are compared against each other (see text for details). High behavioral performance is achieved when dopamine D1 receptor signaling levels in R2/R4m ring neurons are appropriately compared with E-PG D1 activity. This is the case for control and *dumb*^{2} mutant. However, not enough or too much Dop1R1 in R2/R4m ring neurons compared to E-PG neurons lead to poor performances (selective knockdown in wild-type background or selective rescue in *dumb*^{2} heterozygote mutant background). See also Data S1.

DISCUSSION

Freely Moving *Drosophila* Present Preferred Patterns of Activity and Turning Behavior

Using a novel behavioral analysis to investigate action selection and decision-making, we discovered patterns of motor activity and turning behavior in freely moving *Drosophila*. We observed a non-random distribution of IBIs that was comparable to recordings over several days [4]. The burstiness was a strong characteristic of every tested line, with a shape factor κ always <1, indicative of a none-random distribution of IBIs (Figures 1 and 2). These results suggest that scale-invariant temporal pattern of locomotor activity follows a power law distribution seen in fractal behavior [51, 52]. Consistent with a previous report [51], our findings suggest that the EB could act as a central hub coordinating the temporal sequence of motor actions and burstiness and identify specific dopamine D1 receptor signaling as key mediator for their regulation (Figures 3A and 3D).

Additionally, we observed a remarkable pattern of turning behavior when flies approached the arena wall. Our analysis revealed a bimodal distribution of approach angle with peaks of ±70°–80°, irrespective of left and right preference (Figure 1F). Because the turns we investigated occurred within a single uninterrupted bout of activity, the observed turning behavior could reveal a decision-making process. But why do flies prefer to make a turn in such a way? We posit that flies know where they are in relation to the limits of the arena. As turning was measured within a single bout of activity, we hypothesized that flies anticipate the turn they are going to make in order to avoid a collision with the wall [2]. Thus a ±70°–80° turn might represent the most efficient turning approach during a continuous walking bout, independently of activity levels as demonstrated by the *FoxP* mutant results (Figure 2C).

Impaired Temporal Distribution of Motor Activity and Turning Behavior of *FoxP* Mutants Reminiscent of Indecisiveness

Action selection and decision-making processes require the accumulation of perceptual evidences for adaptive behavior, a process previously shown to be impaired in *FoxP* mutants [29, 36]. Indeed, we observed altered motor activity and turning behavior in two well-described *FoxP* mutants [29, 31], *FoxP*$^{5\text{-}SZ\text{-}3955}$ and *FoxP*^{f03746}. Previous studies have shown these mutants to be deficient in a self-learning, but not world-learning, assay, suggesting that self-generated actions are not correctly processed or perceived [31]. These *FoxP* mutants also take more time to decide in an odor discrimination task indicative of decision-making deficits [29]. These behavioral alterations are accompanied by subtle anatomical alterations [31] but also by disrupted synaptic integration, affecting how salient information is added and retained [36]. In our behavioral assay, these *FoxP* mutants showed decreased burstiness associated with increased shape factor κ, revealing an altered temporal distribution of IBIs. Such observations are indicative of an altered action selection process [3, 4]. Additionally, we no longer detected the bimodal distribution of turns. As the measured turning events occurred within a continuous bout of activity, we assume that the difficulty of the task probably resides in the apparent absence of benefit whichever turn is completed and its fast execution, thus making a decision challenging. The changes in the angle approach distribution could be due to the fact that synaptic integration of self-generated and/or sensory cues is perturbed, as it has been shown for self-learning [31] and odor-discrimination tasks [36]. The resulting random distribution of turns in these *FoxP* mutants (Figure 2C) suggests that the action-selection process and the subsequent decision-making are impaired.

Despite these specific behavioral phenotypes, the expression and spatio-temporal activity of *FoxP* in *Drosophila melanogaster* remains unclear. There is no working antibody available, and the expression patterns of different *FoxP-Gal4* drivers highlight different structures. DasGupta and colleagues generated a *FoxP-Gal4* driver that shows restricted expression in the core of the mushroom body (MB), the olfactory learning and memory center [29]. However, Lawton and colleagues generated another *FoxP-Gal4* driver by recombining the putative *FoxP* promoter with *UAS-CD8::GFP* for visualizing the expression pattern of FoxP protein. They found GFP labeling in the PB [30]. The PB is involved in visual and tactile information processing as well as head-direction signaling [7, 53], all of which are necessary for spatial navigation and turning behavior [2, 19, 20]. However, it remains to be shown whether FoxP is indeed active in the PB, especially the E-PG neurons.

E-PG and Tangential Ring Neurons Differentially Modulate Turning Behavior via Circuit-Specific D1 Receptor Signaling

Previous studies suggested that activity of E-PG neurons represent an internal compass that combines external sensory

cues with self-generated cues [2, 19, 20], thus exhibiting properties reminiscent of heading-direction cells [22]. Based on these earlier findings, we first investigated the potential role of D1 signaling in E-PG neurons and found impaired activity levels and a bimodal distribution sharpened around peaks of ±75° turns. *R60D05-Gal* > *Dop1R1* mutant flies spent less time close to the wall of the arena (Figures 3A and S3A), indicative of altered place preference. What could be the role of D1 signaling for turning behavior? Dopamine is a key neuromodulator known to be required for reinforcement signaling, thereby adding value to behaviorally relevant signals [54, 55]. Our results indicate that dopamine D1 receptor signaling modulates the interaction between E-PG and tangential ring neurons, thereby mediating turning behavior and, in a more general sense, decision-making in the fly. This interpretation is consistent with recent models suggesting E-PG and ring neurons constitute a ring attractor that is also involved in an abstract internal representation of the fly's heading direction [50]. Indeed, stimulation experiments [19, 50] and computational modeling [2, 50, 56] suggest that inhibitory GABAergic ring neurons [57] receive excitation from E-PGs and provide reciprocal inhibition back onto E-PGs in wedges of the EB, resulting in global inhibition (ring neurons) among local excitation (E-PGs) [50]. We therefore hypothesize that D1 signaling modulates E-PG and EB R2/4 m circuit activities, which are compared against each other, with E-PG D1 activity coding for a value about the fly's navigational goal in relation to its position in the arena and toward the wall, whereas D1 activity in R2/4 m neurons modulates the weighting of the received input for action selection. The net result of this comparison is a weighted evaluation of the predicted outcome of the fly's next action(s) and its behavioral performance. This model is consistent with the outcome of altered Dop1R1 signaling in *E-PG* > *Dop1R*$^{-RNAi}$ flies, where we observed decreased activity levels and an altered place preference with distribution of turns sharpened around peaks of ±75° turns. These data suggest that Dop1R1 signaling in R60D05 E-PG neurons facilitates motor activity and turning behavior, especially for ±75–0° turns. If D1-specific drivers targeting individual columnar neurons were available, it would be interesting to test this hypothesis.

However, a possible limitation of our investigation is the *R60D05-Gal4* mediated expression of Dop1R1^{-RNAi} in all E-PG neurons, which might be inappropriate to impact turning behavior. Previous experiments by Green et al., using the same Gal4 driver line, revealed that a turn is performed when the activity of a single PB glomerulus takes over the rest of the population, leading to locally restricted neuronal activity [19, 44]. In fact, Green and colleagues showed that rotation of a tethered fly—equivalent to a turn in our assay—can be induced by local activation of 1 or 2 glomeruli only [19]. Thus, Dop1R1-mediated manipulation over the entire R60D05-targeted E-PG neuron population might not have any consequence on the execution of turns. As we could not technically exploit this level of resolution with freely moving animals and investigate this hypothesis in our behavioral assay, we then extended our analysis to tangential ring neurons.

We first validated a computational assumption necessary for spatial navigation [2] and showed reciprocal contacts of potential pre-synaptic termini between E-PG and ring neurons. Even though the physiology of the connections has to be experimentally demonstrated, the observed GFP reconstitution signals support a model where E-PG neurons, integrating visual landmark and heading direction [44], and ring neurons, mediating a selection process likely via ring attractor activity [50], together code for neural mechanisms underlying sensory integration and motor action selection for spatial navigation [2]. Therefore, we wondered how we could efficiently modulate this functional nexus in order to affect turning behavior. More than changing activity levels of ring neurons, we decided to manipulate dopamine D1 signaling, a key modulator of action selection circuitries [9, 37], including the EB [2, 9].

We found a profound effect of D1 signaling specifically in the EB R2/R4m circuitry, which was previously shown to modulate an environmentally induced increase in locomotor activity [25, 41], as well as naive (unconditioned) odor avoidance [58]. Our analysis revealed that impaired D1 signaling in the EB R2/R4m circuitry affected both the temporal distribution of IBIs but also turning behavior. We observed an increase in burstiness and indecision when approaching the wall (Figure 3D). Strikingly, the turning behavior was not due to a general decrease of dopamine D1 receptor levels because *dumb*^{2} mutants were unaffected (Figure 5A). Rather, the observed behavioral phenotypes were specifically caused by a Dop1R1 imbalance localized to the outer layer circuit of the EB, which our results suggest to be reciprocally connected with E-PG neurons (Figure 4). This behavioral observation was confirmed by targeting Dop1R1 in the R2/R4m circuitry in a heterozygous *dumb*^{2} mutant background, although manipulating R1-R3/4d EB circuits was without any measured behavioral consequence (Figure 5). These findings are reminiscent of the inverted-U shape hypothesis of dopamine action and behavioral performance, where both too little and too much dopamine signaling impairs behavioral outcome [59]. We extend this relation to dopamine D1 receptor levels and behavioral performance between interconnected CX circuitry (Figure 6).

A possible alternative explanation though suggests the reported Dop1R1 manipulations lead to a non-functional internal compass. A mismatch between idiothetic and allothetic cues that input on the EB could cause ambiguity in the head-direction (HD) signal and uncertainty in the direction estimate of the fly. The prediction of such a confused HD signal would be random distribution of turns. However, targeting Dop1R^{-RNAi} to the E-PG circuit resulted in a more pronounced bimodal distribution (see Figure 3A), which is the exact opposite of a random distribution of turns. In contrast, targeting Dop1R^{-RNAi} to R2/4 m caused the loss of a bimodal distribution indicative of a random-like distribution of turns. Yet this does not necessarily suggest a confused HD signal, because the R2/4 m circuit has been implicated in sleep pressure and arousal [24–26] as well as memory formation [27, 28, 46, 47, 60], behavioral manifestations difficult to reconcile with only head-direction signaling. The most parsimonious explanation for these different R2/4 m-mediated behavioral manifestations is "shared action selections," even for sleep pressure as suppressed activity. We therefore propose that D1-modulated interaction between E-PG and EB ring neurons is an integral part of the circuits and mechanisms underlying action selection and decision-making in *Drosophila*.

STAR★METHODS

Detailed methods are provided in the online version of this paper and include the following:

- KEY RESOURCES TABLE
- CONTACT FOR REAGENT AND RESOURCE SHARING
- EXPERIMENTAL MODEL AND SUBJECT DETAILS
- METHOD DETAILS
  - Immunohistochemistry
  - Open-field behavioral analysis
  - Kinematic calculations
  - Motor actions
  - Motor action sequences
  - Burstiness behavior
  - Mechanical stimulus response and arousal state
  - Turning Behavior Metrics
  - Radial Distance and Circumferential angle
  - Edge Region
  - Edge Contact
  - Outer Region Crossings
  - Pre/Post-Edge Contact Sequences
  - Approach Angle
  - Overall Fly Location
  - Exploration Percentage
- QUANTIFICATION AND STATISTICAL ANALYSIS
- DATA AND SOFTWARE AVAILABILITY

SUPPLEMENTAL INFORMATION

Supplemental Information includes six figures and one data file and can be found with this article online at https://doi.org/10.1016/j.cub.2019.01.017.

ACKNOWLEDGMENTS

We thank Angelique Lamaze, Katrin Vogt, Manolis Fanto, Bruno van Swinderen, Bassem Hassan, and Thomas Preat for comments on the manuscript and the Wohl Cellular Imaging Centre at King's College London for help with microscopy. We thank the reviewers for constructive criticisms of our initial manuscript. We are grateful to the Miesenbock lab for FoxP reagents and to Scott Waddel for dopamine reagents. This work was supported by an IoPPN-King's Independent Researcher Award to B.K., a PhD fellowship from CAPES Foundation-Ministry of Education of Brazil to J.B. (BEX 13162/13-6), and grants from the BBSRC (BB/N001230/1) and MRC UK (G0701498 and MR/L010666/1) to F.H.

AUTHOR CONTRIBUTIONS

Conceptualization, B.K. and F.H.; Methodology, B.K. and R.F.; Investigations, B.K. and J.B.; Validation, B.K.; Software, R.F.; Writing – Original Draft, B.K.; Writing – Review & Editing, B.K. and F.H.; Funding Acquisition, F.H.; Supervision, B.K. and F.H.

DECLARATION OF INTERESTS

B.K. and R.F. are co-founders of BFK, Ltd. All remaining authors declare no competing interest.

Received: September 14, 2018
Revised: November 29, 2018
Accepted: January 9, 2019
Published: January 31, 2019

REFERENCES

1. Prescott, T.J., Bryson, J.J., and Seth, A.K. (2007). Introduction. Modelling natural action selection. Philos. Trans. R. Soc. Lond. B Biol. Sci. *362*, 1521–1529.
2. Fiore, V.G., Kottler, B., Gu, X., and Hirth, F. (2017). *In silico* interrogation of insect central complex suggests computational roles for the ellipsoid body in spatial navigation. Front. Behav. Neurosci. *11*, 142.
3. Barabási, A.L. (2005). The origin of bursts and heavy tails in human dynamics. Nature *435*, 207–211.
4. Sorribes, A., Armendariz, B.G., Lopez-Pigozzi, D., Murga, C., and de Polavieja, G.G. (2011). The origin of behavioral bursts in decision-making circuitry. PLoS Comput. Biol. *7*, e1002075.
5. Reynolds, A.M. (2011). On the origin of bursts and heavy tails in animal dynamics. Physica A *390*, 245–249.
6. de Bivort, B.L., and van Swinderen, B. (2016). Evidence for selective attention in the insect brain. Curr. Opin. Insect Sci. *15*, 9–15.
7. Heinze, S. (2017). Unraveling the neural basis of insect navigation. Curr. Opin. Insect Sci. *24*, 58–67.
8. Pfeiffer, K., and Homberg, U. (2014). Organization and functional roles of the central complex in the insect brain. Annu. Rev. Entomol. *59*, 165–184.
9. Strausfeld, N.J., and Hirth, F. (2013). Deep homology of arthropod central complex and vertebrate basal ganglia. Science *340*, 157–161.
10. Strauss, R. (2002). The central complex and the genetic dissection of locomotor behaviour. Curr. Opin. Neurobiol. *12*, 633–638.
11. Turner-Evans, D.B., and Jayaraman, V. (2016). The insect central complex. Curr. Biol. *26*, R453–R457.
12. Varga, A.G., Kathman, N.D., Martin, J.P., Guo, P., and Ritzmann, R.E. (2017). Spatial navigation and the central complex: sensory acquisition, orientation, and motor control. Front. Behav. Neurosci. *11*, 4.
13. Donlea, J.M. (2017). Neuronal and molecular mechanisms of sleep homeostasis. Curr. Opin. Insect Sci. *24*, 51–57.
14. Ito, K., and Awasaki, T. (2008). Clonal unit architecture of the adult fly brain. Adv. Exp. Med. Biol. *628*, 137–158.
15. Lin, C.Y., Chuang, C.C., Hua, T.E., Chen, C.C., Dickson, B.J., Greenspan, R.J., and Chiang, A.S. (2013). A comprehensive wiring diagram of the protocerebral bridge for visual information processing in the Drosophila brain. Cell Rep. *3*, 1739–1753.
16. Wolff, T., Iyer, N.A., and Rubin, G.M. (2015). Neuroarchitecture and neuroanatomy of the Drosophila central complex: a GAL4-based dissection of protocerebral bridge neurons and circuits. J. Comp. Neurol. *523*, 997–1037.
17. Strausfeld, N.J. (2012). Arthropod Brains: Evolution, Functional Elegance and Historical Significance (Harvard University Press).
18. Seelig, J.D., and Jayaraman, V. (2013). Feature detection and orientation tuning in the Drosophila central complex. Nature *503*, 262–266.
19. Green, J., Adachi, A., Shah, K.K., Hirokawa, J.D., Magani, P.S., and Maimon, G. (2017). A neural circuit architecture for angular integration in Drosophila. Nature *546*, 101–106.
20. Seelig, J.D., and Jayaraman, V. (2015). Neural dynamics for landmark orientation and angular path integration. Nature *521*, 186–191.
21. Green, J., and Maimon, G. (2018). Building a heading signal from anatomically defined neuron types in the Drosophila central complex. Curr. Opin. Neurobiol. *52*, 156–164.
22. Heinze, S. (2015). Neuroethology: unweaving the senses of direction. Curr. Biol. *25*, R1034–R1037.
23. Giraldo, Y.M., Leitch, K.J., Ros, I.G., Warren, T.L., Weir, P.T., and Dickinson, M.H. (2018). Sun navigation requires compass neurons in Drosophila. Curr. Biol. *28*, 2845–2852.e4.
24. Donlea, J.M., Pimentel, D., and Miesenböck, G. (2014). Neuronal machinery of sleep homeostasis in Drosophila. Neuron *81*, 860–872.
25. Lebestky, T., Chang, J.S., Dankert, H., Zelnik, L., Kim, Y.C., Han, K.A., Wolf, F.W., Perona, P., and Anderson, D.J. (2009). Two different forms

of arousal in Drosophila are oppositely regulated by the dopamine D1 receptor ortholog DopR via distinct neural circuits. Neuron *64*, 522–536.

26. Liu, S., Liu, Q., Tabuchi, M., and Wu, M.N. (2016). Sleep Drive Is Encoded by Neural Plastic Changes in a Dedicated Circuit. Cell *165*, 1347–1360.
27. Kuntz, S., Poeck, B., Sokolowski, M.B., and Strauss, R. (2012). The visual orientation memory of Drosophila requires Foraging (PKG) upstream of Ignorant (RSK2) in ring neurons of the central complex. Learn. Mem. *19*, 337–340.
28. Ofstad, T.A., Zuker, C.S., and Reiser, M.B. (2011). Visual place learning in Drosophila melanogaster. Nature *474*, 204–207.
29. DasGupta, S., Ferreira, C.H., and Miesenböck, G. (2014). FoxP influences the speed and accuracy of a perceptual decision in Drosophila. Science *344*, 901–904.
30. Lawton, K.J., Wassmer, T.L., and Deitcher, D.L. (2014). Conserved role of Drosophila melanogaster FoxP in motor coordination and courtship song. Behav. Brain Res. *268*, 213–221.
31. Mendoza, E., Colomb, J., Rybak, J., Pflüger, H.J., Zars, T., Scharff, C., and Brembs, B. (2014). Drosophila FoxP mutants are deficient in operant self-learning. PLoS ONE *9*, e100648.
32. Faville, R., Kottler, B., Goodhill, G.J., Shaw, P.J., and van Swinderen, B. (2015). How deeply does your mutant sleep? Probing arousal to better understand sleep defects in Drosophila. Sci. Rep. *5*, 8454.
33. Besson, M., and Martin, J.R. (2005). Centrophobism/thigmotaxis, a new role for the mushroom bodies in Drosophila. J. Neurobiol. *62*, 386–396.
34. Fisher, S.E., and Scharff, C. (2009). FOXP2 as a molecular window into speech and language. Trends Genet. *25*, 166–177.
35. Haesler, S., Rochefort, C., Georgi, B., Licznerski, P., Osten, P., and Scharff, C. (2007). Incomplete and inaccurate vocal imitation after knockdown of FoxP2 in songbird basal ganglia nucleus Area X. PLoS Biol. *5*, e321.
36. Groschner, L.N., Chan Wah Hak, L., Bogacz, R., DasGupta, S., and Miesenböck, G. (2018). Dendritic Integration of Sensory Evidence in Perceptual Decision-Making. Cell *173*, 894–905.e13.
37. Cisek, P., and Kalaska, J.F. (2010). Neural mechanisms for interacting with a world full of action choices. Annu. Rev. Neurosci. *33*, 269–298.
38. Alekseyenko, O.V., Chan, Y.B., Li, R., and Kravitz, E.A. (2013). Single dopaminergic neurons that modulate aggression in Drosophila. Proc. Natl. Acad. Sci. USA *110*, 6151–6156.
39. Kim, Y.C., Lee, H.G., Seong, C.S., and Han, K.A. (2003). Expression of a D1 dopamine receptor dDA1/DmDOP1 in the central nervous system of Drosophila melanogaster. Gene Expr. Patterns *3*, 237–245.
40. Kim, Y.C., Lee, H.G., and Han, K.A. (2007). D1 dopamine receptor dDA1 is required in the mushroom body neurons for aversive and appetitive learning in Drosophila. J. Neurosci. *27*, 7640–7647.
41. Kong, E.C., Woo, K., Li, H., Lebestky, T., Mayer, N., Sniffen, M.R., Heberlein, U., Bainton, R.J., Hirsh, J., and Wolf, F.W. (2010). A pair of dopamine neurons target the D1-like dopamine receptor DopR in the central complex to promote ethanol-stimulated locomotion in Drosophila. PLoS ONE *5*, e9954.
42. Riemensperger, T., Isabel, G., Coulom, H., Neuser, K., Seugnet, L., Kume, K., Iché-Torres, M., Cassar, M., Strauss, R., Preat, T., et al. (2011). Behavioral consequences of dopamine deficiency in the Drosophila central nervous system. Proc. Natl. Acad. Sci. USA *108*, 834–839.
43. Ueno, T., Tomita, J., Tanimoto, H., Endo, K., Ito, K., Kume, S., and Kume, K. (2012). Identification of a dopamine pathway that regulates sleep and arousal in Drosophila. Nat. Neurosci. *15*, 1516–1523.
44. Green, J., Vijayan, V., Mussells Pires, P., Adachi, A., and Maimon, G. (2018). Walking Drosophila aim to maintain a neural heading estimate at an internal goal angle. bioRxiv. https://doi.org/10.1101/315796.
45. Keleman, K., Vrontou, E., Krüttner, S., Yu, J.Y., Kurtovic-Kozaric, A., and Dickson, B.J. (2012). Dopamine neurons modulate pheromone responses in Drosophila courtship learning. Nature *489*, 145–149.
46. Neuser, K., Triphan, T., Mronz, M., Poeck, B., and Strauss, R. (2008). Analysis of a spatial orientation memory in Drosophila. Nature *453*, 1244–1247.
47. Pan, Y., Zhou, Y., Guo, C., Gong, H., Gong, Z., and Liu, L. (2009). Differential roles of the fan-shaped body and the ellipsoid body in Drosophila visual pattern memory. Learn. Mem. *16*, 289–295.
48. Feinberg, E.H., Vanhoven, M.K., Bendesky, A., Wang, G., Fetter, R.D., Shen, K., and Bargmann, C.I. (2008). GFP Reconstitution Across Synaptic Partners (GRASP) defines cell contacts and synapses in living nervous systems. Neuron *57*, 353–363.
49. Macpherson, L.J., Zaharieva, E.E., Kearney, P.J., Alpert, M.H., Lin, T.Y., Turan, Z., Lee, C.H., and Gallio, M. (2015). Dynamic labelling of neural connections in multiple colours by trans-synaptic fluorescence complementation. Nat. Commun. *6*, 10024.
50. Kim, S.S., Rouault, H., Druckmann, S., and Jayaraman, V. (2017). Ring attractor dynamics in the *Drosophila* central brain. Science *356*, 849–853.
51. Martin, J., Faure, P., and Ernst, R. (2001). The power law distribution for walking-time intervals correlates with the ellipsoid-body in Drosophila. J. Neurogenet. *15*, 205–219.
52. Cole, B.J. (1995). Fractal time in animal behavior: the movement activity of Drosophila. Anim. Behav. *50*, 1317–1324.
53. Ritzmann, R.E., Harley, C.M., Daltorio, K.A., Tietz, B.R., Pollack, A.J., Bender, J.A., Guo, P., Horomanski, A.L., Kathman, N.D., Nieuwoudt, C., et al. (2012). Deciding which way to go: how do insects alter movements to negotiate barriers? Front. Neurosci. *6*, 97.
54. Berke, J.D. (2018). What does dopamine mean? Nat. Neurosci. *21*, 787–793.
55. Guitart-Masip, M., Duzel, E., Dolan, R., and Dayan, P. (2014). Action versus valence in decision making. Trends Cogn. Sci. *18*, 194–202.
56. Kakaria, K.S., and de Bivort, B.L. (2017). Ring attractor dynamics emerge from a spiking model of the entire protocerebral bridge. Front. Behav. Neurosci. *11*, 8.
57. Kottler, B., Fiore, V.G., Ludlow, Z.N., Buhl, E., Vinatier, G., Faville, R., Diaper, D.C., Stepto, A., Dearlove, J., Adachi, Y., et al. (2017). A lineage-related reciprocal inhibition circuitry for sensory-motor action selection. bioRxiv. https://doi.org/10.1101/100420.
58. Li, W., Cressy, M., Qin, H., Fulga, T., Van Vactor, D., and Dubnau, J. (2013). MicroRNA-276a functions in ellipsoid body and mushroom body neurons for naive and conditioned olfactory avoidance in Drosophila. J. Neurosci. *33*, 5821–5833.
59. Birman, S. (2005). Arousal mechanisms: speedy flies don't sleep at night. Curr. Biol. *15*, R511–R513.
60. Wang, Z., Pan, Y., Li, W., Jiang, H., Chatzimanolis, L., Chang, J., Gong, Z., and Liu, L. (2008). Visual pattern memory requires foraging function in the central complex of Drosophila. Learn. Mem. *15*, 133–142.
61. Lin, S., Owald, D., Chandra, V., Talbot, C., Huetteroth, W., and Waddell, S. (2014). Neural correlates of water reward in thirsty Drosophila. Nat. Neurosci. *17*, 1536–1542.

STAR★METHODS

KEY RESOURCES TABLE

REAGENT or RESOURCE	SOURCE	PurPose
Antibodies		
rabbit anti-GFP 1:500	ThermoFisher Scientific A6455	Gal4 characterization
mouse anti-GFP 1:200	Sigma-Aldrich G6539	GRASP signal
goat anti-mouse Alexa fluor 488, 1:150	Life Technologies - A11031	Secondary antibody
goat anti-rabbit Alexa fluor 488, 1:150	Life Technologies - A11034	Secondary antibody
Experimental Models: Organisms/Strains		
Drosophila: EB1-Gal4	[57]	R2/R4m specific driver
Drosophila: C232-Gal4	[57]	R3/D4d specific driver
Drosophila: C105-Gal4	[57]	R1 specific driver
Drosophila: R60D05-Gal4	[20]	E-PG specific driver
Drosophila: Dop1R1-RNAi	[61]	Dopaminergic D1-like receptor RNAi
Drosophila: Dumb2 mutant	[61]	Dopaminergic D1-like receptor mutant
Software and Algorithms		
DART software for recording	[32]	Behavioral recording
DART software for analysis	This paper	Behavioral analysis

CONTACT FOR REAGENT AND RESOURCE SHARING

Further information and requests for resources and reagents should be directed to and will be fulfilled by the Lead Contact, Dr. Frank Hirth (frank.hirth@kcl.ac.uk.)

EXPERIMENTAL MODEL AND SUBJECT DETAILS

Flies were maintained on a 12:12 light:dark cycle at 18°C and were grown standard cornmeal medium. Two days after eclosion, flies were anesthesized with CO2, separated and kept at 25°C for at least 2 days until the experiment. Except for Figure 1 which compares genders, all experiments used mated females. The following strains were used: w^{1118} as control flies, *c105-Gal4*, *c232-Gal4*, *EB1-Gal4*. For GRASP experiments we combined *EB1-Gal4* and *R60D05-LexA* from the Janelia collection. The Aop-CD4::spGFP11; *UAS*-syb::spGFP1-10 or Aop-syb::spGFP1-10; *UAS*-CD4::spGFP11 [49] were generous gifted from the Jepson lab. $Dumb^2$ line and UAS-Dop1R-^{RNAi} (VDRC ID 107058 = KK102341) were generous gifts from Scott Waddell. The FoxP, $FoxP^{5\text{-}SZ\text{-}3955}$ and $FoxP^{f03746}$ mutants were generous gifts from Gero Miesenbock.

METHOD DETAILS

Immunohistochemistry

Brains were dissected in cold PBS and fixed for 1hr at room temperature in 4% (wt/vol) paraformaldehyde in PBS (130 mM NaCl, 7 mM Na2HPO4, 3 mM KH2PO4), followed by three 10-min washes in PBT (PBS containing 0.5% Triton X-100). Brains were then blocked in PBT plus 2% (wt/vol) NGS for 20-min, and incubated overnight at 4°C with the primary antibodies diluted in the same solution at 4°C. The primary antibodies were mouse anti-GFP (ThermoFisher Scientific 33-2600, 1:500 for msGFP detection or Sigma-Aldrich G6539, 1:200 for reconstituted splitGFP detection). The secondary antibodies were goat anti-mouse and anti-rabbit conjugated to Alexa fluor 488 or 555 (Invitrogen Molecular Probes, 1:150). For *R60D05-Gal4* > *UAS-mCD8::GFP* brains, no anti-GFP antibody was used. This was followed by three 10-min washes in PBT, 2-h incubation with the secondary antibodies at room temperature, three 20-min washes in PBT again, and one final wash in PBS. Tissues were mounted in Vectashield (Vector Laboratories). Images were acquired with a Nikon A1R confocal microscope equipped with 40x 1.3NA Plan Fluor oil immersion objective, processed using the Fiji software and Figure constructed in Adobe Illustrator.

Open-field behavioral analysis

Fly tracking was performed using custom-made platforms made of Acetal copolymer (POM-C), Tecaform AH. A platform comprises 36 open-field arenas, each arena 35mm in diameter and 1.5mm height, all covered with a transparent acrylic sheet with 1mm holes for

breathing. The platform with arenas was placed on a white light plate that provided uniform cold light illumination within a temperature-controlled incubator (Stuart Scientific). Only females where taken unless mentioned otherwise. Flies were transferred individually into each arena after a short cold anesthesia and left to acclimatize for at least 30 minutes. Video-assisted motion tracking and analyses were carried out using the DART system [32] with custom-made MATLAB (Mathworks) scripts. Video recordings were carried out using a Logitech c920 camera at 10 frames per second for 1 hour. The positions of flies were extracted every 2 recorded frames (effective average interframe duration = 0.20 s).

Kinematic calculations

To determine locomotion parameters, we calculated fly motion as follows: The inter-frame displacement, D_i (which is calculated between the i^{th} and $(i\text{-}1)^{th}$ video frames) is calculated using the following equation:

$$D_i = \sqrt{(X_i - X_{i-1})^2 + (Y_i - Y_{i-1})^2} \quad \text{(Equation 1)}$$

where X_j/Y_j denote the X/Y coordinates (respectively) for frame j. The inter-frame speed is calculated using Equation 1 as follows:

$$V_i = D_i/(T_i - T_{i-1}) \quad \text{(Equation 2)}$$

where T_j denotes the time stamp for frame j. The activity threshold of a fly: a fly is considered "active" for a given video frame if Equation 2 exceeds 2mm/sec, which is equivalent to the traveling the body length of the fly every second.

Motor actions

The *percentage activity* is calculated as the percentage of video frames during which the fly is active. This data is also shown in a *raster plot* that depicts activity bouts during 60 minutes of recording, with black vertical lines representing active frames and white space representing inactive frames the duration of which depicts the inter-bout intervals (IBIs). *Traces:* plots showing the track of each individual fly during the first 10 minutes of recording within the corresponding genotypic group. *Activity/min*: activity levels for each animal were calculated and were then averaged over all other recorded flies (per genotype) to obtain the mean *activity/min*. *Speed* was calculated by averaging Equation 2 for each video frame over all flies per genotype. *Distance* was calculated by summing Equation 1 over all active frames for each fly (during the 60 minutes of recording), and then averaged over all recorded flies per genotype.

Motor action sequences

Action initiation was defined as the number of times a fly transitions from an inactive to active state divided by the total time spent inactive. This metric is averaged over all recorded flies per genotype to give the mean number of activity bouts started per second. *Mean bout length* was defined as the duration for which an individual fly remains continuously active. Measures are averaged over all recorded flies per genotype. *Interbout interval* (IBI) is the duration for which a fly is continuously inactive; the minimum IBI is 0.2 s, which corresponds to an averaged inter-frame duration. This metric is averaged over all recorded flies per genotype to give the mean duration of an IBI as pause.

Burstiness behavior

Animal activity is characterized by burstiness, which characterizes burst of activity in a short time window followed by extensive periods of inactivity [3–5]. Burstiness can be described by a Weibull distribution, which calculates the cumulative distribution of inter-bout intervals (IBIs) of a given group of animals (here a genotype) during a defined period of time, here during the 60min window of recording. To quantify the IBI distribution, survival curves were fit using a Weibull distribution with the following functional form:

$$y = e^{-(x/\lambda)^{\kappa}} \quad \text{(Equation 3)}$$

where x is the IBI, λ is the scale factor, and κ is the shape factor. Using this Weibull distribution, λ and κ can be deduced that reflects the degree of burstiness for a given group. A shape factor κ of 1 corresponds to a random distribution (Poisson) of IBIs whereas its decrease corresponds to an increase in burstiness behavior, that is: burst of activity are no longer randomly distributed but occur in clusters.

In order to estimate the parameters λ and κ, Equation 3 is linearized by using the transform $\overline{y} = log_e(-log_e(y))$ and $\overline{x} = log_e(x)$ such that:

$$\overline{y} = \kappa\overline{x} + c \quad \text{(Equation 4)}$$

where $c = -\kappa log_e(\lambda)$. From Equation 4, the parameters λ and κ were estimated using the MATLAB optimization function, *fit* (Mathworks).

Mechanical stimulus response and arousal state

A mechanical stimulation was delivered after 30 minutes of recording and was composed of 5 vibrations at 3 Volts for 200ms separated by 800ms. Mechanical stimulation and response analyses were carried out as previously described [32]. The pre-stimuli speed represents the average speed of all flies per genotype 2 minutes prior to mechanical stimulation (calculated using Equation 2). The

absolute post-stimuli speed is calculated again using Equation 2, but is smoothed (so as to remove high-frequency noise) using the following equation:

$$\widehat{V}_i \approx \left(\sum_{j=0}^{N_{Avg}-1} V_{i-j} \right) \Big/ N_{Avg} \quad \text{(Equation 5)}$$

where N_{Avg} is the number preceding video frames (N_{Avg} = 10). The final absolute post-stimuli speed trace is determined by interpolating Equation 5 to the nearest second. From the post-stimuli speed trace, the amplitude is calculated as the difference between the maximum stimuli response and the average pre-stimuli speed. To quantify the features of the stimuli response, the relative post-stimuli signal (calculated as the absolute post-stimuli speed minus the average pre-stimuli speed) is fitted with a single-inactivation exponential equation with the following functional form:

$$V(\tau) = \left(1 - e^{-\tau/\tau_A}\right)\left(A_0 + A_1 e^{-\tau/\tau_{I1}}\right)H(\tau) \quad \text{(Equation 6)}$$

where $\tau = t - \delta t$, $H(\tau)$ is the Heaviside step function (= 1 if $\tau > 0$, otherwise 0), $A_{0\text{-}2}$ are scale factors, τ_A is the activation time constant, and τ_A/τ_{I1} are inactivation time constants. The exponential equation parameters (the scale factors, time constants and δt) for Equation 6 were fitted using the MATLAB optimization function, *fit* (Mathworks).

Turning Behavior Metrics

In order to extract the distribution of approach angles, several parameters are considered:

Movement Threshold $\leq$ 2mm/sec. The speed at which a fly is considered moving.
Circumferential Distance = 2mm. The circumferential threshold distance for determining movement after edge contact. The circumferential distance is the distance the fly travels around the circular region (as opposed to radially)
Pre-edge Contact Duration = 2 s. The active duration before contact with the wall used to determine the approach angle.
Post-edge Contact Duration = 2 s. The active duration after contact with the wall used to determine edge behavior.
Minimum Edge Contact = 1 s. Minimum duration the fly has to be in the outer ring to be considered as edge region.
Outside Edge Distance = 3mm. The distance from outside edge whereby the fly is considered in contact with wall.

Radial Distance and Circumferential angle

A fly position has the following coordinates at a given time $T_{(i)}$ over an experiment of n_{Frm} Frames: ($X_{(i)}$, $Y_{(i)}$). The radial distance and circumferential angle are denoted, respectively, by $\rho_{(i)} = D(X_{(i)}, Y_{(i)})$ and $\varphi_{C(i)} = \omega(X_{(i)}, Y_{(i)})$ where:

$$D(X,Y) = \sqrt{X^2 + Y^2} \quad \text{(Equation 7)}$$

$$\omega(X,Y) = \tan^{-1}(Y/X) \quad \text{(Equation 8)}$$

Edge Region

We define the "edge region" of the circle to be the annulus formed by the circle's edge and an inner circle of radius (R-ΔR). The distance R-(R-ΔR) is manually established within the DART program at 3mm.

Schematic diagram illustrating regions and other definitions

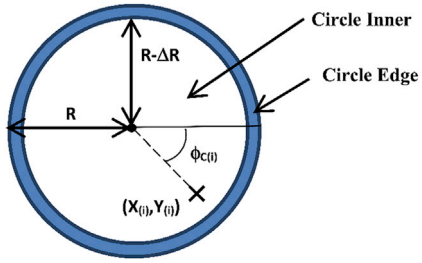

Edge Contact

A fly is considered to be within the circle's edge region if the following is true:

$$(R - \Delta R) < \rho_{(i)} < R \quad \text{(Equation 9)}$$

Given this is true, a valid edge contact event is said to have occurred if the fly remains in the outer region for at least T_{min}, or in terms of video frames:

$$n_{min} = T_{min} \times n_{FPS} \quad \text{(Equation 10)}$$

where n_{FPS} is video frame rate and equals 5 frame/sec. From this, video frames are given a designation of 1 if that frame constitutes a valid edge contact (0 otherwise) and is denoted by the symbol, $Z_{(i)}$. It follows that the proportional duration that the fly spends in the outer region, denoted by P_{out}, is calculated as follows:

$$P_{Out} = \frac{\sum_i Z_{(i)}}{n_{Frm}} \quad \text{(Equation 11)}$$

Outer Region Crossings

Given the valid edge contact events are known, it is trivial to determine the times at which the fly enters/leaves the outer region (after a valid contact event) which has cardinality n_{out}/n_{in}, respectively. Therefore, the total number of edge crossings is given by:

$$n_{Cross} = n_{out} + n_{in} - 1 \quad \text{(Equation 12)}$$

Pre/Post-Edge Contact Sequences

In order to calculate the approach angle the pre-edge contact sub-sequence is formed by taking the n_B frames preceding $\xi_{(j)}$. Conversely, the post-edge contact behavioral metrics are determined from the sub-sequences formed from the n_A frames subsequent to $\xi_{(j)}$. The values of n_B/n_A are linked to the video frame rate by the equation:

$$n_X = T_X \times n_{FPS} \quad (\text{where } X = A \text{ or } B) \quad \text{(Equation 13)}$$

where T_B/T_A is the pre/post-contact duration, respectively. Note that for an edge contact to be considered valid for the metric calculations, the following must be true:

$$\xi_{(1)} > n_B \quad \text{(Equation 14)}$$

$$\left(\xi_{(j+1)} - \overline{\xi}_{(j)}\right) > n_B \quad \text{(Equation 15)}$$

$$\xi_{\left(n_{edge}\right)} < (n_{Frm} - n_A) \quad \text{(Equation 16)}$$

$$\left(\xi_{(j+1)} - \xi_{(j)}\right) > (n_B + n_A) \quad \text{(Equation 17)}$$

In other words, there must be at least A) n_B frames before the start of the first edge contact event, B) n_B frames between a fly leaving and re-entering the edge region, C) n_A frames subsequent to the final edge contact event, and D) $(n_A + n_B)$ frames between the start of contact events.

Approach Angle

The positional coordinates of the pre-edge contact sub-sequences are rotated with respect to $\varphi_{(\xi_{(j)})}$ (i.e., the circumferential angle from the frame where the fly first crosses into the edge contact region):

$$\text{i.e., } \begin{bmatrix} \overline{X}_{(k)} \\ \overline{Y}_{(k)} \end{bmatrix} = \begin{bmatrix} \cos\varphi_{(\xi_{(j)})} & \sin\varphi_{(\xi_{(j)})} \\ -\sin\varphi_{(\xi_{(j)})} & \cos\varphi_{(\xi_{(j)})} \end{bmatrix} \begin{bmatrix} X_{\left(\xi_{(j)}+(k-(n_B+1))\right)} \\ Y_{\left(\xi_{(j)}+(k-(n_B+1))\right)} \end{bmatrix} \quad \text{(Equation 18)}$$

where $k = 1$ to n_B+1. The approach angle (denoted by $\phi_{A(j)}$) is calculated from the rotated coordinates by taking the distance weighted sum of the inter-frame angles as follows:

$$\varphi_{A(j)} = \sum_{l=1}^{n_B} W_{(l)}\omega\left(\overline{X}_{(l+1)} - \overline{X}_{(l)}, \overline{Y}_{(l+1)} - \overline{Y}_{(l)}\right) \quad \text{(Equation 19)}$$

$$W_{(l)} = \frac{Q_{(l)}}{\sum_{m=1}^{n_B} Q_{(m)}} \quad \text{(Equation 20)}$$

$$Q_{(l)} = \frac{1}{D\left(\overline{X}_{n_B+1} - \frac{\overline{X}_l + \overline{X}_{l+1}}{2}, \overline{X}_{n_B+1} - \frac{\overline{Y}_l + \overline{Y}_{l+1}}{2}\right)} \quad \text{(Equation 21)}$$

In other words, the inter-frame angles are weighted by calculating the distance from the average position between adjacent frames to the final frame in the sub-sequence (i.e., the frame where the fly enters the edge region). This means that inter-frame angles that are closer to the edge region have a higher weighting. Negative approach angles denote that the fly is approaching the edge from the left side, and positive angles approaching from the right.

Note that only the frames where the fly is continuously moving toward the arena edge are considered for the approach angle calculation (i.e., $(\overline{X}_{(l+1)} - \overline{X}_{(l)}) > 0$). Furthermore, for the metric analysis, the approach angles are separated into bins of size $\Delta\phi$ from a domain of -90° to 90°. In our analysis, we choose a resolution of 5degrees. This leads to plotting histogram value (y axis value) in function of orientation bin angle (x axis value). The fitted line on the distribution follows a bimodal log-normal distribution equation using the MATLAB optimization function, *fit* (MathWorks)

$$f(\varnothing) = \frac{A}{\sigma\sqrt{2\pi}}\left(\frac{e^{\frac{-(log_e(\varnothing)-\mu)^2}{2\sigma^2}}}{\varnothing} + \frac{e^{\frac{-(log_e(180-\varnothing)-\mu)^2}{2\sigma^2}}}{180-\varnothing}\right) \quad \text{(Equation 22)}$$

Where A is the shape factor, μ is the mean, s is the standard deviation and ϕ is the approach angle (A, μ and $\sigma > 0$, $-180^\circ < \phi < 180^\circ$)

For the polar plot graphical representation of the turning preference, each histogram is normalized to the maximum Y-value. This way the longest value reaches the outside of the circle and all other values are relative to this maximum and we can plot a vector length representing the average turning event.

Overall Fly Location

This is the ratio of the frames where the fly is within the edge region to the total number of frames:

$$P_{Loc} = \frac{\sum_{j=1}^{n_{Edge}}\left(\overline{\xi}_{(j)} - \xi_{(j)}\right)}{n_{Frm}} \quad \text{(Equation 23)}$$

Exploration Percentage

To determine the percentage of the open-field region that the fly explores during the duration of the experiment, the positional coordinates are converted from pixels to mm as follows:

$$\widehat{X}_{(i)} = X_{(i)}/S_F \quad \text{(Equation 24)}$$

$$\widehat{Y}_{(i)} = Y_{(i)}/S_F \quad \text{(Equation 25)}$$

Where S_F is the pixel to mm scale factor, which for our experiments, was usually on the order of 0.35 mm/pixel. From these converted positional coordinates, the locations of the fly between each frame is estimated by linear interpolation and rounded to the nearest pixel (integer) value. Given the number of unique locations, from the known and interpolated positional values which are denoted by n_{Tot}, the exploration percentage is given by the equation:

$$E = \frac{n_{Tot}}{Area} = n_{Tot}\pi\left(\frac{S_F}{R}\right)^2 \quad \text{(Equation 26)}$$

QUANTIFICATION AND STATISTICAL ANALYSIS

For the histograms, each dataset was tested for normality using the Anderson-Darling test with $\alpha = 0.05$. If every dataset under comparison was normal and the variances were similar (a ratio of 4 between the highest and lowest variance was used as the cut-off), then a one-way ANOVA test was used to determine whether any differences existed between groups. If significance was found for ANOVA with $\alpha = 0.05$, then pairwise comparisons were carried out using a post hoc Tukey-Kramer test, again with $\alpha = 0.05$. If any of the datasets was found not to be normally distributed, then a Kruskal-Wallis test was used to determine any overall differences between the groups with $\alpha = 0.05$. If significance was achieved, a post hoc pairwise Mann-Whitney U test with Dunn-Sidak correction was used to compare groups with $\alpha = 0.05$. For each test group, two controls were used. All calculations were performed using MATLAB within

the DART software. For testing the significance of changes in the bimodal distribution of approach angles, we first pooled together turns of similar absolute values, assuming that conceptually a right or a left turn is the same. We then performed two sample Kolmogorov-Smirnov (KS) tests on the normalized data to the maximum between the experimental and the two parental controls to evaluate alteration in the distribution of approach angles. Significance was achieved when the experimental was statistically different from the two controls, and that no difference was observed between controls. All data were extracted from the DART software and KS tests were run in Graph Pad 7.04. In all Figures, the p value of the statistical test is represented as either one star ($p < 0.05$), two stars ($p < 0.01$) or three stars ($p < 0.001$).

DATA AND SOFTWARE AVAILABILITY

Data supporting the findings of this study are available within the paper and its Supplemental Information files and from the authors upon request.

Current Biology, Volume *29*

Supplemental Information

Inverse Control of Turning Behavior by Dopamine D1 Receptor Signaling in Columnar and Ring Neurons of the Central Complex in *Drosophila*

Benjamin Kottler, Richard Faville, Jessika Cristina Bridi, and Frank Hirth

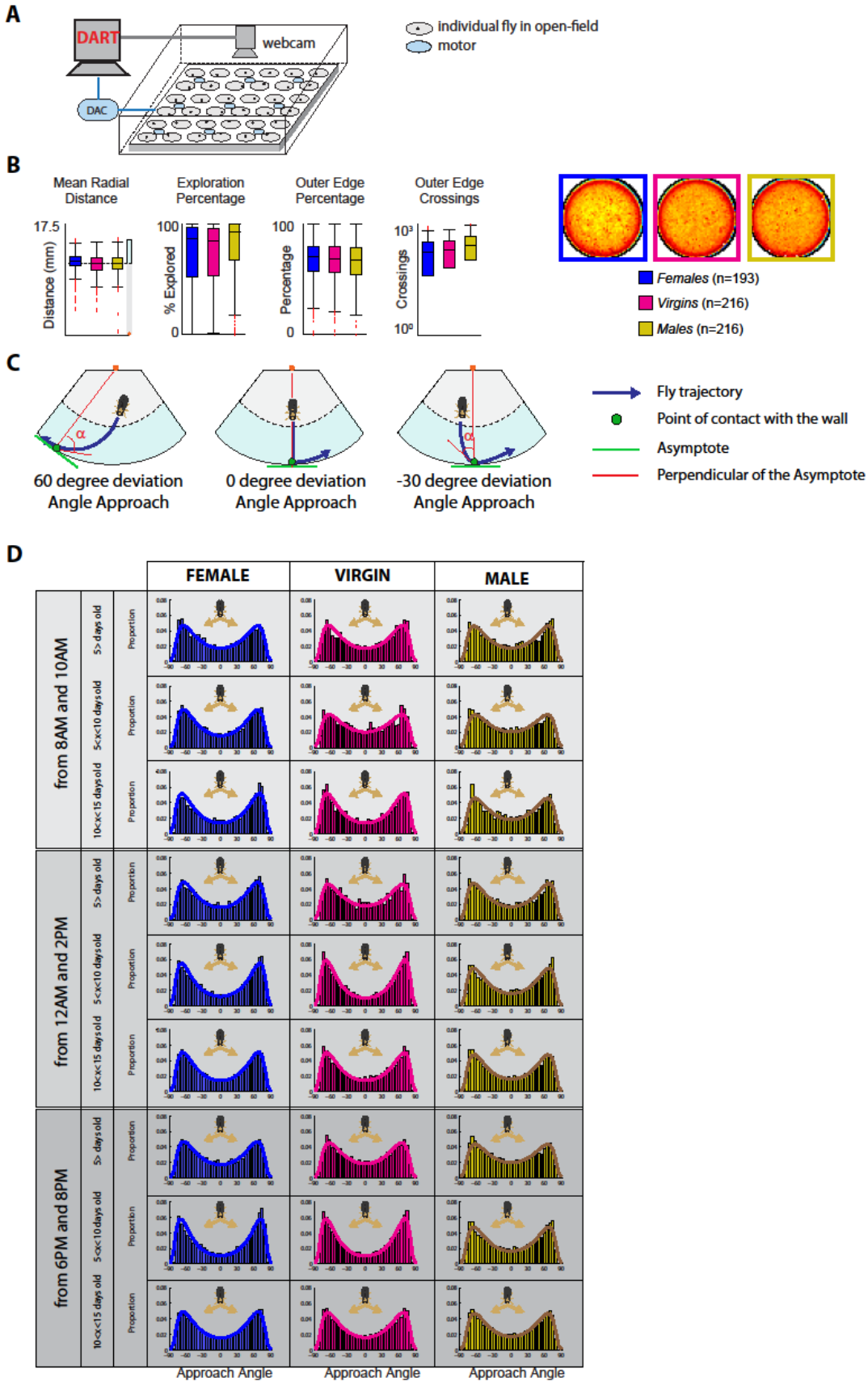
A
DART
webcam
DAC
individual fly in open-field
motor
B
Mean Radial Distance
Exploration Percentage
Outer Edge Percentage
Outer Edge Crossings
17.5
Distance (mm)
100
% Explored
0
100
Percentage
0
10³
Crossings
10⁰
Females (n=193)
Virgins (n=216)
Males (n=216)
C
60 degree deviation Angle Approach
0 degree deviation Angle Approach
-30 degree deviation Angle Approach
Fly trajectory
Point of contact with the wall
Asymptote
Perpendicular of the Asymptote
D
FEMALE
VIRGIN
MALE
from 8AM and 10AM
from 12AM and 2PM
from 6PM and 8PM
5> days old
5<x<10 days old
10<x<15 days old
Proportion
Approach Angle

Figure S1: Open-field behaviour of freely moving controls flies. Relates to Figure 1. (**A**) Behavioural setup; platform with 36 open-field arenas, each hosting one fly, placed in a temperature-controlled incubator; all experimental and control flies were tracked at the same time. DART software was used for controlling the webcam and the motor, via a digital to analogue converter (DAC); motor activation elicits a vibration shock. (**B**) Place preference metrics for control groups, w^{1118} females, virgins and males. (**C**) Schematics of turning behaviour: left, the fly approaches the edge making a sharp clockwise turn to the its right; middle, the fly walks straight to the wall making the turn after contact; right, the fly makes a slight counter clock turn. (**D**) Gender comparison across time of the day and age. Mated females (in blue), virgin females (in pink) and males (in yellow) were compared at different time points of the day and age. In every case, the bimodal distribution is presented with peaks at -/+70degrees and there is no statistical difference between groups.

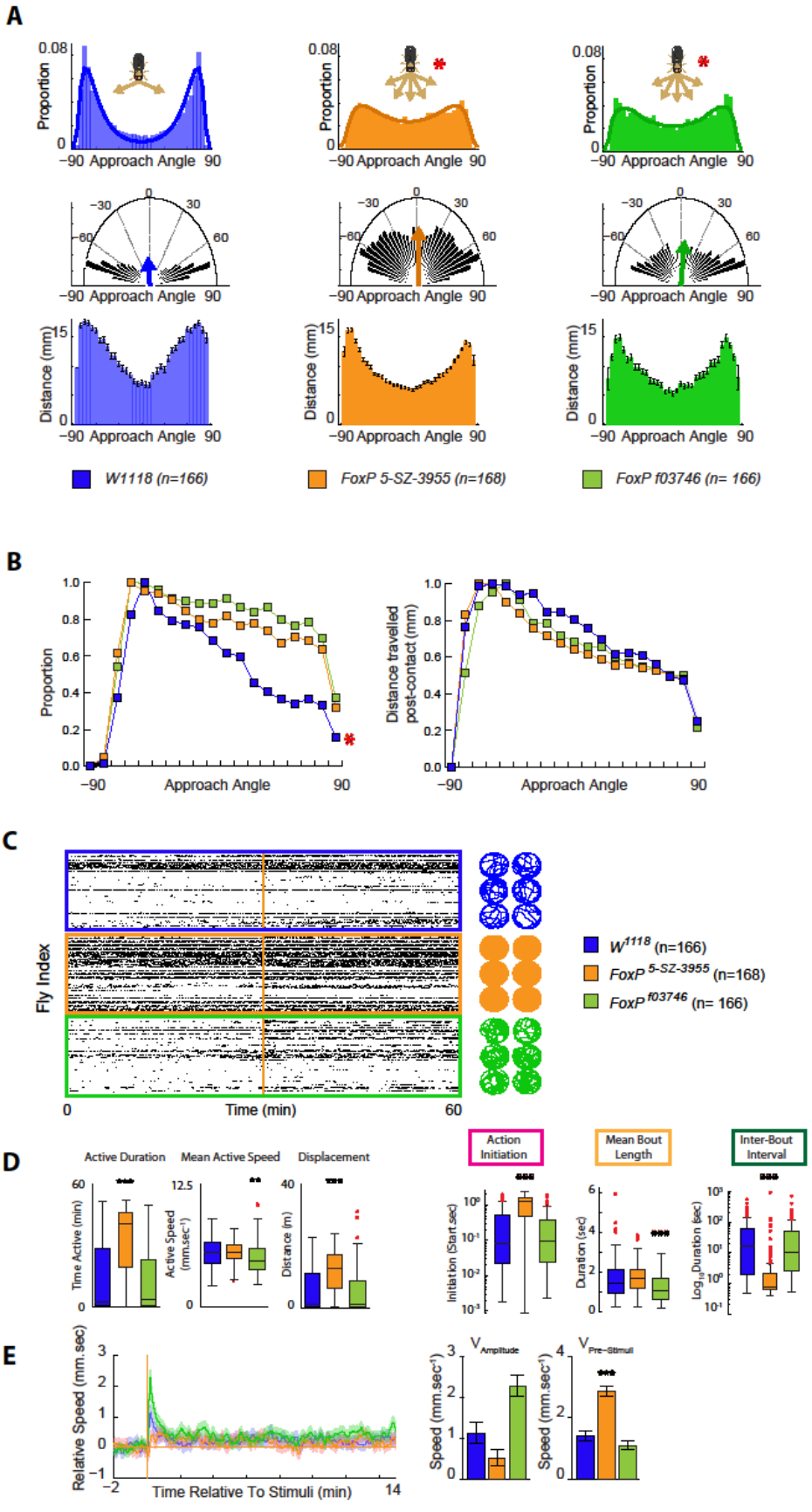
A
Proportion
0.08
0
−90 Approach Angle 90
−30
30
−60
60
0
Distance (mm)
15
W1118 (n=166)
FoxP 5-SZ-3955 (n=168)
FoxP f03746 (n= 166)
B
Proportion
Approach Angle
Distance travelled post-contact (mm)
C
Fly Index
Time (min)
0
60
W1118 (n=166)
FoxP 5-SZ-3955 (n=168)
FoxP f03746 (n= 166)
D
Active Duration
Mean Active Speed
Displacement
Time Active (min)
Active Speed (mm.sec⁻¹)
Distance (m)
Action Initiation
Mean Bout Length
Inter-Bout Interval
Initiation (Start sec)
Duration (sec)
Log10Duration (sec)
E
Relative Speed (mm.sec)
Time Relative To Stimuli (min)
V Amplitude
V Pre-Stimuli
Speed (mm.sec⁻¹)

Figure S2: Locomotor kinematics and open-field behaviour of freely moving *FoxP* mutant flies. Relates to Figure 2. (**A**) approach angle distribution, polar plot representation, and distance travelled post contact with the wall for each group w^{1118} (blue), $FoxP^{5\text{-}SZ\text{-}3955}$ (orange) and $FoxP^{f03746}$ (green) females. (**B**) Left, each approach angle proportion have been grouped based on absolute value and normalized to the maximum; right each distance travelled postcontact with the edge have been grouped based on absolute value and normalized to the maximum. The asterisk represents significant difference with the two other groups based on two sample Kolmogorov-Smirnov (KS). (**C**) Raster plot activity of w^{1118} (blue), $FoxP^{5\text{-}SZ\text{-}3955}$ (orange) and $FoxP^{f03746}$ (green) females; trajectories recorded for the first 10 minutes; panels of the right show activity metrics, mean activity of flies (active duration), their mean active speed (middle) and the distance they walked during the recordings (Displacement). (**D**) Activity metrics related for 60 min recording. (**E)** Relative speed over time before and after stimuli (dashed orange line) are applied; panels on right show stimuli response as amplitude of increased speed after stimuli and pre-stimuli speed. All data are mean +/- SEM; *p<0.5, **p<0.01, ***p<0.001.

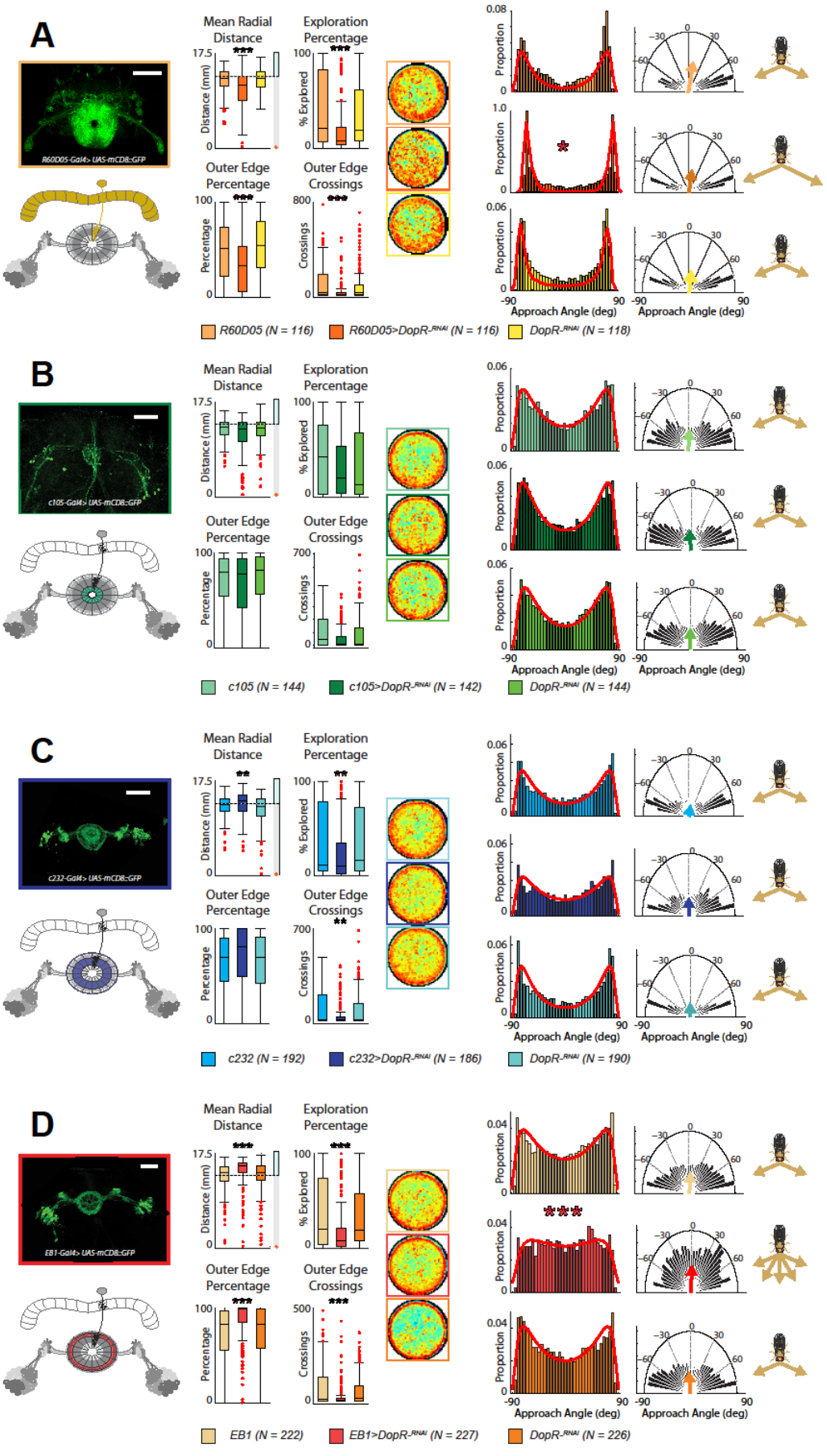
A
R60D05-Gal4> UAS-mCD8::GFP
Mean Radial Distance
Exploration Percentage
Outer Edge Percentage
Outer Edge Crossings
Distance (mm)
% Explored
Percentage
Crossings
Proportion
Approach Angle (deg)
R60D05 (N = 116)
R60D05>DopR-RNAi (N = 116)
DopR-RNAi (N = 118)
B
c105-Gal4> UAS-mCD8::GFP
c105 (N = 144)
c105>DopR-RNAi (N = 142)
DopR-RNAi (N = 144)
C
c232-Gal4> UAS-mCD8::GFP
c232 (N = 192)
c232>DopR-RNAi (N = 186)
DopR-RNAi (N = 190)
D
EB1-Gal4> UAS-mCD8::GFP
EB1 (N = 222)
EB1>DopR-RNAi (N = 227)
DopR-RNAi (N = 226)

Figure S3. *Dop1R1-*^{RNAi} expression affects open field exploration and turning behaviour in an ellipsoid body circuit-specific manner. Relates to Figure 3. (**A**) *R60D05-Gal4>Dop1R1-* ^{RNAi} place preference metrics and heatmap on the left; right turning behaviour for *R60D05-Gal4* control *R60D05-Gal4>Dop1R1-* ^{RNAi} and *Dop1R1-* ^{RNAi} control (**B**) *c105-Gal4>Dop1R1-* ^{RNAi} place preference metrics and heatmap on the left; right turning behaviour for *c105-Gal4* control, *c105-Gal4>Dop1R1-* ^{RNAi} and *Dop1R-* ^{RNAi} control. (**C**) *c232-Gal4>Dop1R1-* ^{RNAi} place preference metrics and heatmap on the left; right turning behaviour for *c232-Gal4* control, *c232-Gal4>Dop1R1-* ^{RNAi} and *Dop1R1-* ^{RNAi} control. (**D**) *EB1-Gal4>Dop1R1-* ^{RNAi} place preference metrics and heatmap on the left; right turning behaviour for *EB1-Gal4* control, *EB1-Gal4>Dop1R1-* ^{RNAi} and *Dop1R1-* ^{RNAi} control. All data are mean +/-SEM; *p<0.5, **p<0.01, ***p<0.001. Scale bar 50μm.

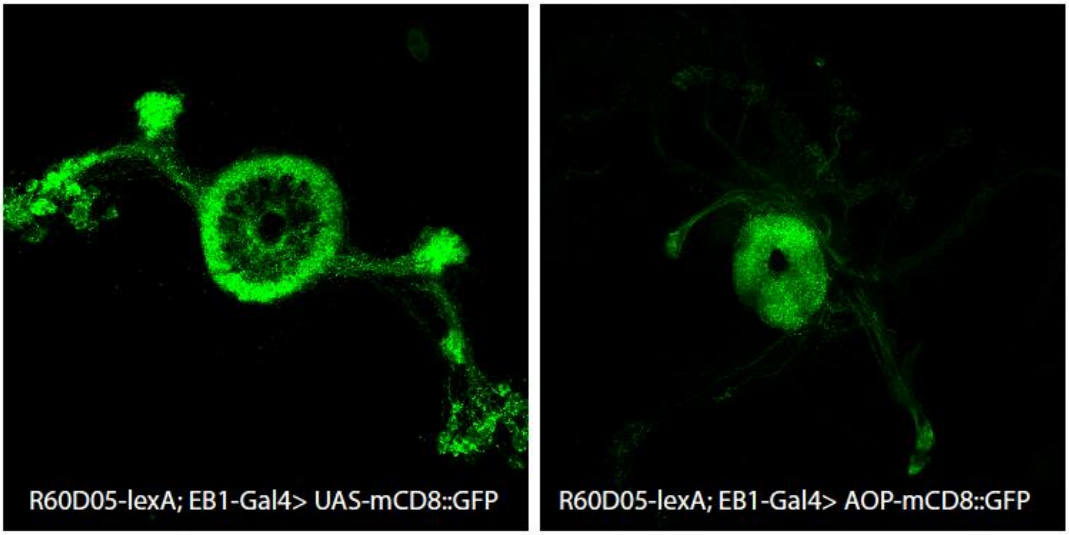

Figure S4. Brain-specific expression pattern of founder lines used for synaptobrevin-tagged Green fluorescent protein *reconstitution across* columnar wedge and tangential ring neurons. Relates to Figure 4. (Left) *R60D05-lexA; EB1-Gal4>UAS-mCD8::GFP* expression pattern highlight the ring neurons R2/R4m. (Right) *R60D05-lexA; EB1-Gal4>AOP-mCD8::GFP* highlight the columnar-wedge neurons innervating the ellipsoid body**.**

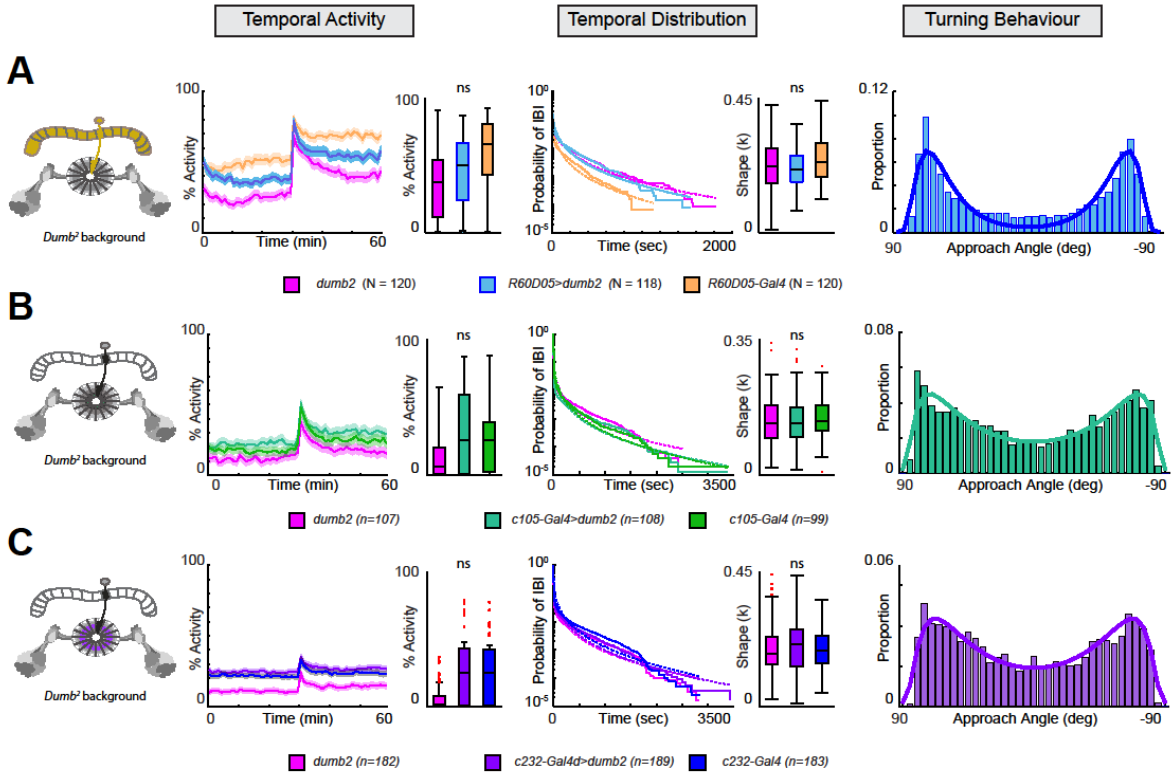

Figure S5. DopR1 receptor mutant Dumb2 affects activity levels but not temporal distribution of activity bouts or turning behaviour. Relates to Figure 5. Panels from left to right indicate DopR1 levels in entire brain and/or ring neuron subtype-specific ellipsoid body (EB) circuitry; temporal activity levels; mean activity; temporal distribution of inter-bout intervals (IBIs); shape factor κ of burstiness; distribution of approach angle for (**A**) *dumb*^{2} mutant compared to columnar-wedge specific driver *R60D05-Gal4* restoring Dop1R1 in *dumb*^{2} heterozygous background and *R60D05-Gal4* control flies (**B**) *Dumb*^{2} mutant compared to R1-specific *c105-Gal4* targeting Dop1R1 in *dumb*^{2} heterozygous background and *c105-Gal4* control flies; (**C**) *Dumb*^{2} mutant compared to R3/4d-specific *c232-Gal4* restoring Dop1R1 in *dumb*^{2} heterozygous background and *c232-Gal4* control flies. All data are mean +/-SEM; *p<0.5, **p<0.01, ***p<0.001.

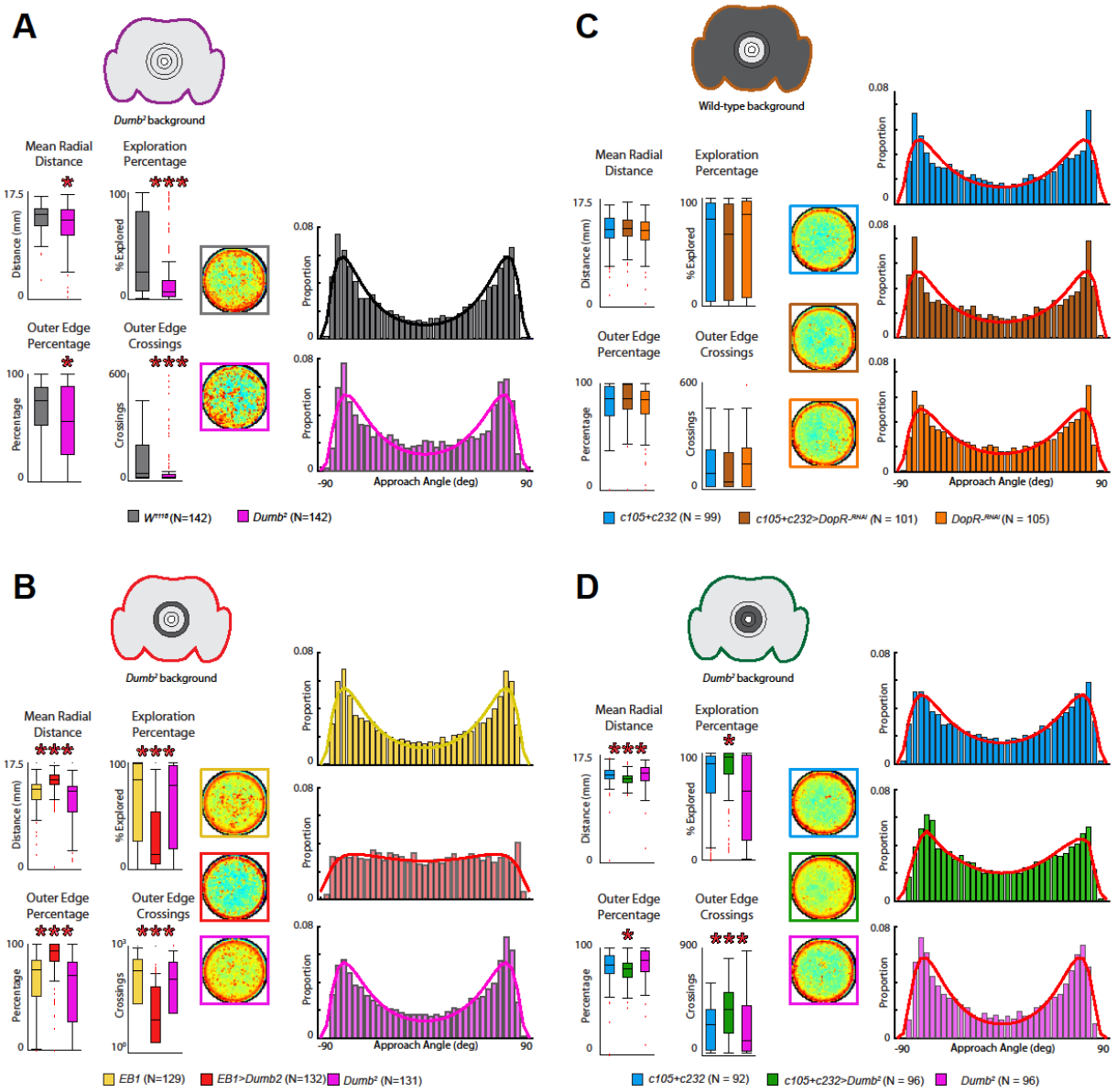

Figure S6. Place preference and exploration metrics for Dopaminergic manipulations. Relates to Figure 5. (A) *Dumb*^{2} place preference metrics and heatmap on the left shows less centrophobism; approach angle distributions between *w11118* and *dumb*^{2} on the right are not different. (**B**) R2/R4m specific *EB1-Gal4* restoring Dop1R1 in *dumb*^{2} heterozygous background show less centrophobism, less exploration and less transition from outer to inner edge region; right, altered turning behaviour for *EB1-Gal4> dumb*^{2}. (**C**) left, place preference metrics and heatmap for *c105-Gal4-c232-Gal4> Dop1R1-* ^{RNAi} and turning behaviour on the right. (**D**) left, place preference metrics and heatmap for *c105-Gal4-c232-Gal4> dumb*^{2} show a statistically significant decrease in centrophobism whereas turning behaviour, on the right, is not affected. All data are mean +/-SEM; *p<0.5, **p<0.01, ***p<0.001. Grey background represents low level of Dop1R1, whereas a darker background shows normal level of expression.